Utrecht University

Utrecht University - Faculty of Geosciences

MSc Science and Innovation - ENERGY SCIENCE

Academic year 2018-2019

Master Thesis

Advancing technology and data modelling for optimisation of non-dispatchable renewable electricity coupled with underground H_2 storage

Supervisor:
Dr. Matteo Gazzani
Co-supervisor:
Lukas Weimann MSc

Author:
Annika Boldrini
ID num. 6253768

Abstract

Intermittent power generation is a considerable obstacle to the integration of wind and solar energy into the electrical grid. To compensate for the seasonal intermittency of wind velocity and solar radiation, large-scale energy storage is required that must be capable of storing energy on a monthly time-scale. Therefore, the feasibility of hydrogen storage in salt caverns coupled to wind and solar power production is analysed. A Mixed-Integer Linear Programming (MILP) optimisation is performed within the boundaries of the Dutch electrical grid by applying the aforementioned technologies. This research is performed in the context of an existing MILP tool. The optimal design and operation is analysed in variation of the methods applied for weather profile modelling. The MILP tool calls for hourly weather data on a one-year time horizon. Three methodologies are developed for the creation of a Typical Meteorological Year (TMY) from a long-term weather database; their performances and impact are tested on the Dutch case-study. On the one hand, optimal design determines maximum deployment of wind and solar technologies for all scenarios, with area constraints playing a key role; on the other hand, the optimal system operations highly differ, for instance as respect to trade-off between offshore and onshore power production. Nevertheless, hydrogen storage is deployed on a negligible scale; copious amount of electricity is curtailed rather than stored. The tool is applied with continuous curtailment, which is found to hinder the actual potential of the large renewable capacity installed. To conclude, opportunity for enhancement of the developed methods are reported.

Keywords: MILP, large-scale energy storage, wind energy, solar energy, typical meteorological year

Acknowledgements

I would like to thank Matteo Gazzani, whose expertise, dedication and continuous support have made my experience throughout these months engaging, gratifying and an endless source of learning. I would also like to thank Lukas Weimann, whose limitless support has been essential during all the stages of my research. Last but not least, a special thank goes to my parents, my role models and pillars, whose love and guidance have allowed me to reach this accomplishment.

Annika Boldrini

Utrecht, 15th of March 2019

Contents

List of Figures

List of Tables

Nomenclature

EP Expected Profile, page 12

ES Expected Spikes, page 14

KNMI Koninklijk Nederlands Meteorologisch Instituut, page 8

MES Multi-Energy System, page 1

MILP Mixed-Integer Linear Programming, page I

NDRES Non Dispatchable Renewable Energy Resources, page 1

OSN Offshore Node, page 25

PEME Proton Exchange Membrane Electrolyser, page 24

PEMFC Proton Exchange Membrane Fuel Cell, page 23

PN Province Node, page 25

PtG Power to Gas, page 1

PV Photovoltaic, page 2

RD Representative Days, page 12

SCN Salt Cavern Node, page 25

TMY Typical Meteorological Year, page I

Chapter 1

Introduction

The Paris Agreement addresses the urgency to limit the global average temperature increase to 1.5°C above pre-industrial levels [Rhodes, 2016]; thereafter the European Commission set targets for each member state to reach: CO_2 emissions reduction of at least 40% by 2030 and 80% by 2050, in comparison to 1990 levels, together with a 27% share of renewable energy by 2030 [Hof et al., 2012]. Accordingly, renewable energy is being extensively deployed in the Netherlands. Albeit the 14% share of renewable energy target for 2020 is unlikely to be achieved [European Commission, , ECN,], large renewable energy deployment is planned for the next decade; as for government scheme, 3500 MW of offshore wind capacity is expected to be installed by 2023, adding to the 1000 MW currently installed; additional 7000 MW of wind capacity is planned by 2030 [The Ministry of Infrastructure and the Environment, 2014]. On the other hand, the integration of non dispatchable renewable energy resources (NDRES; wind and solar) represents a challenge for its stability and reliability, due to their intermittent nature. Current studies show that the power grid can only integrate up to 20% of energy produced by wind without storage. Its deployment is then crucial to absorb intermittent generation [Castillo and Gayme, 2014]. The potential of various types of storage technologies implemented in the power system operations are well known [Hadjipaschalis et al., 2009, Díaz-González et al., 2012, Ribeiro et al., 2001]. However, only large-scale energy storage has the potential to provide the required flexibility at grid level, to compensate for the seasonal variation of NDRES [Castillo and Gayme, 2014]. On this account, hydrogen is gaining interest in the role of energy carrier due to its capacity to be stored to a degree of GWh of electrical energy on time scale of weeks or even months [Ozarslan, 2012, Michalski et al., 2017]. In the context of this study, hydrogen is produced from water via electrolysis, with the excess electricity produced by NDRES; then, it is stored in underground salt caverns, in the north-east of the Netherlands. The hydrogen carrier is subsequently used as clean fuel for power production with the use of fuel cells. The production and re-conversion of hydrogen is henceforth called Power to Gas system (PtG).

To achieve a cleaner and more affordable energy system, Mancarella [Mancarella, 2014] highlights the necessity of detaching from a traditional separation between energy sectors. In fact, he shows how the integration of multiple energy carriers, or multi-energy system (MES), allows improvements on the energy system as technical, economic and environmental performances. However, an appropriate optimisation of MES is case specific, because energy systems can widely differ in boundaries and applications. Nevertheless, the concept of MES always analyses the interaction of various energy carriers from demand to generation [Mancarella, 2014]. The concept of *energy hub* has been developed to model generic MES from a technical point of view; *energy hub* is a type of MES aggregation with an input-output perspective, where supply and demand are coupled with the aim of cost minimisation [Mancarella, 2014]. A decentralised energy system can be described by multiple hubs, interacting with each other through energy networks.

The modelling of such systems requires advanced techniques which enable integrated optimisation of design and operation for multiple energy carriers. MILP represents the state-of-the-art mathematical framework for optimisation of energy systems [Weimann et al., 2019]. Recent studies have applied MILP frameworks for the optimisation of multi carriers, distributed energy hubs [Gabrielli et al., 2018, Morvaj et al., 2016, Shao et al., 2017]. As a matter of fact, the adoption of binary variables well captures typical features of energy systems, such as discrete technology deployment, while maintaining the reasonable computational complexity of linear programming [Gabrielli et al., 2018]. The coupling of NDRES and energy storage has been analysed with the use of MILP frameworks in various applications. Marnay *et al.* [Marnay et al., 2008] and Hawkes *et al.* [Hawkes and Leach, 2009] analyse optimal design and operation of residential centralised micro-grids, whilst Wouters *et al.* [Wouters et al., 2015] evaluate multiple decentralised micro-grids for the South Australian residential sector, as well as Mehleri *et al.* [Mehleri et al., 2013] for different Greek neighbourhoods. More researches have been conducted on national level; Pudjanto *et al.* [Pudjianto et al., 2014] investigate the value of grid-scale electricity storage in the UK, by means of minimising investment and operation costs. Samsatli *et al.* [Samsatli et al., 2015] apply a MILP framework to investigate wind turbines deployment on national scale with surplus electricity used for hydrogen production to supply the transport sector. Michalski *et al.* [Michalski et al., 2017] and Welder *et al.* [Welder et al., 2018] examine hydrogen application in PtG systems for power production, the former examines the potentials and economics of salt caverns storage in Germany and the latter shows the advantages of a decentralised wind-hydrogen energy system. Although, they both apply a linear programming approach.

This research is performed in the context of the MILP framework developed by Gabrielli *et al.* [Gabrielli et al., 2018], which calls for hourly weather data on a one-year time horizon. The unpredictability of weather profiles advocates for particular focus on the creation of appropriate TMY. Methods for weather profile modelling have been previously analysed; Wilks *et al.* [Wilks and Wilby, 1999] analyse various stochastic models that also considers weather profiles generators; Guan [Guan, 2009] discusses methods to forecast hourly resolution weather profiles for simulations on built environment; whereas Yang *et al.* [Yang et al., 2003] focus on weather variability affecting grid scale energy production, by calculating the probability of no-supply from solar photovoltaic (PV) and wind power in Hong Kong.

1.1 Research question

The presented study aims at assessing the interaction between wind turbines, solar PV panels, hydrogen storage and hydrogen production and conversion, adjoining the advantages brought by a MILP framework to the previous researches. Through the application of the MILP framework developed by Gabrielli *et al.* [Gabrielli et al., 2018], this research intends to answer to: *What are appropriate methods for constructing a TMY from a long-term database, and how do the created weather profiles influence the optimal deployment and operation of the aforementioned NDRES with large-scale storage on the Dutch electricity grid?* Table 1.1 reports the sub-questions that are carried out throughout data analysis and results examination of the Dutch application. Also, shortcomings of the models, for TMY generation and the EHub, and improvement potential are determined throughout the process.

In the following, the MILP framework applied is briefly described, together with the optimisation solver algorithm. In Part I, the impact of weather profiles variation is firstly tested and three methodologies for the use of the long-term database in creating TMY are reported. In Part II, these are applied to the Dutch electricity grid with the MILP framework EHub; the results of optimal design and operation of the system are reported with focus on choice of TMY method. Finally, the overall limitations of the

study are discussed and conclusions are given.

Table 1.1: Research sub-questions to carry out for the Dutch case-study.

Input data	Results analysis
• Which are exemplar wind turbine model for installations? • What are the representative costs for technologies? Are economies of scale applicable? • What are land and sea constraints for technology deployment?	• How does technology deployment variate with area constraints? • What is the trade-off between onshore and offshore wind farms installations? • what is the optimal exchange of energy between the network nodes? • To what degree is the storage system capable of compensating for the seasonal intermittency? • To what extent is the Netherlands capable of achieving electric autarky and what are the eventual limitations?

Chapter 2

Theoretical Framework

MILP is the most advanced mathematical framework for energy system optimisation [Weimann et al., 2019]. However, the hourly resolution on a one-year time horizon requires the application of typical design days or weeks, to decrease the computational complexity. Nevertheless, Gabrielli *et al.* [Gabrielli et al., 2018] define an approach that allows the use of hourly input data while drastically simplifying the computational complexity; the operation variables are separated into two groups, those related to binary variables and those not related. The former are reduced in number by adopting typical design days, while the latter are defined for every hour of the year. Consequently, the framework developed is able to optimise both design and operation of MES within a reasonable computational time, while adopting weather and energy demand data with hourly resolution on a one-year time horizon.

The following section provides a brief overview of the main equations governing the MILP framework developed by Gabrielli *et al.* (i.e. the EHub) [Gabrielli et al., 2018]. First, the formulation of the optimisation problem is reported; then, focus is given to the *Branch and Bound* method applied by the optimisation solver *Gurobi*.

2.1 The EHub

The primary target of the EHub is to deliver hourly the energy demanded by the end users, by means of the resources available in loco or via grid. The input data of the EHub concerns weather profiles, energy demand, energy prices, current energy mix and emissions; the model reports on output technology selection and size, and details on the operation of the units installed. In the designing of decentralised energy system, multiple hubs may interact through networks for diverse energy carriers.

2.1.1 Problem formulation

The objective function of the optimisation problem aims at the minimisation of the total annual costs J, sum of capital cost J_c, operation cost J_o and maintenance cost J_m, respectively

$$J_c = \sum_{i \in \mathscr{M}} (\lambda_i S_i + \mu_i)\omega_i \tag{2.1}$$

$$J_o = \sum_{j \in \mathscr{N}} \sum_{i \in \mathscr{M}} \sum_{t=1}^{T} (u_{j,t} U_{j,i,t} - v_{j,i,t} V_{j,i,t})\Delta t \tag{2.2}$$

$$J_m = \sum_{i \in \mathscr{M}} \psi_i J_{c,i} \tag{2.3}$$

where λ and μ are the variable and fixed cost coefficients for the i-th technology of the set $\mathscr{M}$, S represents the unit size, ω_i is the annuity factor, used to determine the equivalent annual investment cost with an interest rate of 6%. In Eq. 2.2, u and v indicate import and export prices and the corresponding imported or exported powers U and V for the j-th energy carrier and time instant t. Finally, the annual maintenance cost is given by the fraction ψ of the capital cost J_c.

Alongside the primary objective, the model may confine the annual CO_2 emissions under a maximum threshold; emissions are calculated as:

$$e = \sum_{j \in \mathscr{N}} \varepsilon_j \left(\sum_{i \in \mathscr{M}} \sum_{t=1}^{T} U_{j,i,t} \Delta t \right) \tag{2.4}$$

where ε_j is the specific CO_2 emission of carrier j.

The constraints of the optimisation problem are of two types: (2.5) *Performance of conversion and storage technologies*, describing the performances of the selected technologies; and (2.6) *MES energy balances*, which assure the overall system balance for each carrier by imposing the sum of imported and generated power equal to the exported and consumed, at all stages.

$$S_i^{min} a_i \leq S_i \leq S_i^{max} a_i \tag{2.5}$$

$$\sum_{i \in \mathscr{M}} (U_{j,i,t} + P_{j,i,t} - V_{j,i,t} - F_{j,i,t}) - L_{j,t} = 0 \tag{2.6}$$

where S_i indicates the unit size of the technology i and the binary variable $a_1 \in \{0, 1\}$ determines whether the i-th technology is installed; U is the imported energy, P the generated energy, V the exported energy, F the absorbed energy and L the energy demanded by the end users. More detailed equations are reported by [Gabrielli et al., 2018].

2.1.2 Branch and Bound

After establishing the optimisation boundaries, the resulting MILP is solved using Gurobi v8.02. Such MILPs are typically solved with a branch and bound algorithm, which is explained in the following [Gurobi,].

Starting from the original MILP, *Root* in Figure 2.1, the solver removes all the integrality restrictions from the problem, thus performing the so-called *linear-programming relaxation* of the original MIP. After solving the linear optimisation, the binary variables of the original MILP are here set as integer; as shown in Figure 2.1, the *branching variable* v, whose value in the LP relaxation is a fractional between 3 and 4, is then restricted to be $v \leq 3.0$ and $v \geq 4.0$; two sub-problems are created which are solved using the same procedure and whose solution could be optimal to the original problem. The solver continues the process until the leaves of the *search tree*[1] can either be disposed for unfeasibility or solved while satisfying the original MILP integrality constraints. The latter leaf is designated as *fathomed* node and it does not require further branching. Also, if the fathomed node has the best solution found at that point, it will be called *incumbent*, otherwise it can be discarded. For a minimisation problem, the current incumbent represents the upper bound of the optimal solution of the original MIP (green in Figure 2.1). Instead, the lower bound is the minimum optimal objective value of all of the leaf nodes (light blue in Figure 2.1). Finally, optimality of the solution is demonstrated when the gap between upper and lower bounds approaches zero.

[1] the nodes that have not been branched yet.

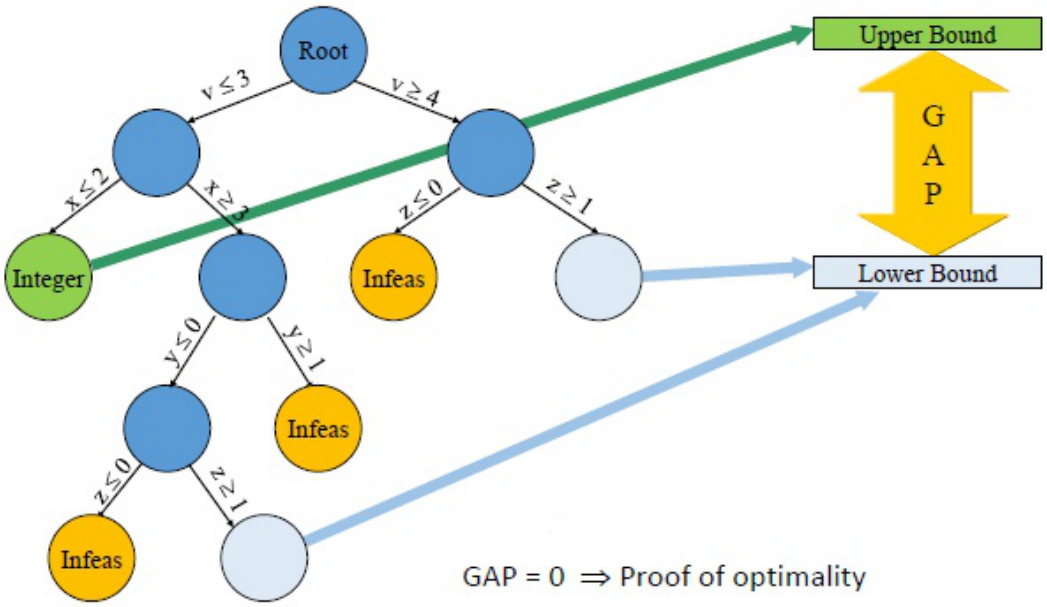

Figure 2.1: Schematic representation of LP based Branch-and-Bound algorithm [Gurobi,].

Part I

Dealing with uncertainties of weather profiles

Chapter 3

Problem definition

An appropriate modelling of NDRES highly depends on weather conditions. The *Koninklijk Nederlands Meteorologisch Instituut* (KNMI) database [KNMI, b, KNMI, a] offers hourly weather data for 35 weather stations in the Netherlands, from the year 1951 until today. For the optimisation of the Dutch electrical grid, data concerning wind speed and solar radiation are required. Problems may arise when a certain year is randomly selected, which may result inappropriate due to anomalous or atypical weather conditions. Figure 3.1 shows the variability of wind speed. Figure 3.1a depicts the wind speeds recorded for a randomly selected a winter hour, the 10th of the year, whilst Figure 3.1b represents a randomly selected summer hour, the 4380th of the year. The reported data are recorded by the weather station *280 Eelde*, located in the province of Drenthe. No consistency or trends are found. The values in Figure 3.1 are categorised to define the frequency distribution of the set of data (i.e. the observed values of a variable to the number of times each value occurs). Since the wind speed is a continuous type of data, it is discretised by categorising the data in ranges, specifically 25 ranges between 0 and 25 m/s. The histograms represented in Figure 3.2 show that the probability distribution derived from the set of data has the shape of a normal distribution, further establishing the unpredictability of the profiles. Therefore, it is necessary to generate one customised year which is representative for the database of all the available years; the TMY [Zang et al., 2012]. The methods for generating a TMY, described in the current chapter, shall be tested in Part II.

As previously mentioned, projects for the implementation of new wind parks in the Netherlands are considerable, therefore the choice of appropriate wind speed profiles to model is crucial; so, the following analysis focuses on wind data and it is later extended to solar radiation. Also, the data analysed henceforth refers to the Drenthe province. Each value of the long-term database is calculated as the mean between data of the same year and hour, recorded from the various weather stations located in the province; they are reported in Appendix A.

First, a brief explanation of wind turbine technology is provided; secondly, an analysis of the extent to which the choice of wind speed profiles influences the wind turbine deployment is presented and finally, three options for generating a TMY are provided.

3.1 Wind turbine technology

Wind turbine electricity generators are manufactured worldwide with capacities ranging from tens of watt to currently 12 MW [Twidell and Weir, 2015]. This renewable energy technology has experienced a rapid onshore growth since the early nineties, developing offshore during the following decade, in waters up to 50 m deep [Twidell and Weir, 2015]. The most common wind turbines have horizontal axis and three blades, which can reach up to 107 m length [Hal,]. The working principle is based on the perturbation

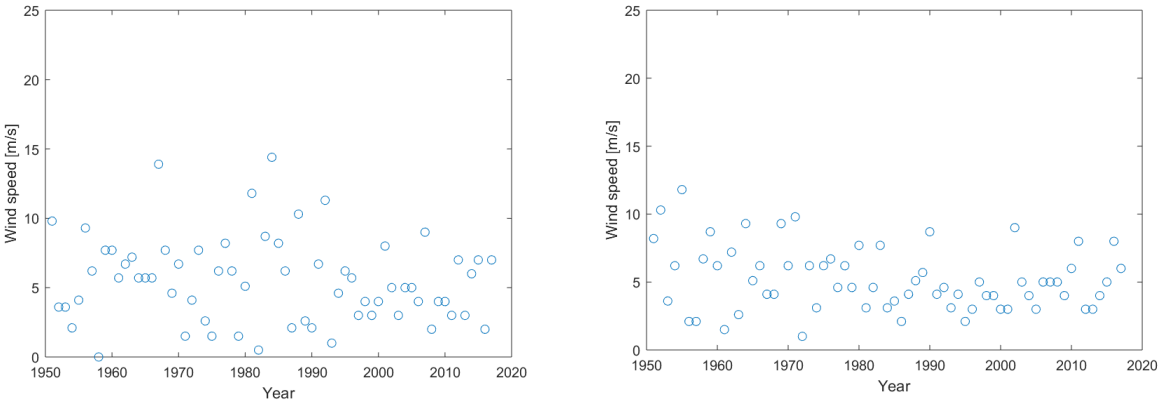

(a) (b)

Figure 3.1: Wind speed for hour 10 (a) and for hour 4380 (b) of the year, from 1951 to 2017 recorded by the weather station 280 in the Drenthe province [KNMI, b].

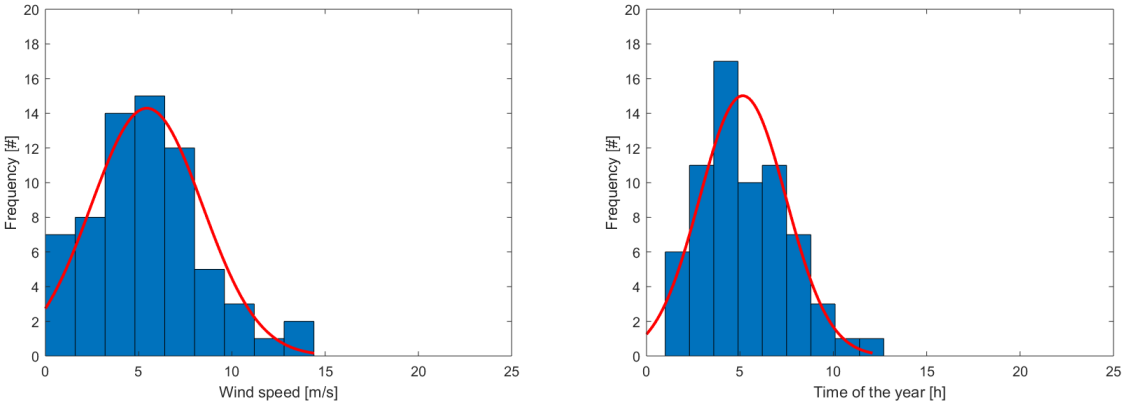

(a) (b)

Figure 3.2: Histogram representing the probability distribution of wind speed data for hour 10 (a) - mean = 5.50 m/s, σ = 3.05 m/s - and hour 4380 (b) - mean = 5.15 m/s, σ = 2.31 m/s - of the year, for data from 1951 to 2017 recorded by the weather station 208 in the Drenthe province.

caused by the blade on the air flow, which cause the generation of Drag and Lift forces on the blades, thus granting their mechanical rotation. The wind turbine rotor is connected to the main shaft, which spins a generator to generate electricity [Twidell and Weir, 2015].

Wind turbines manufacturers must supply measured operating power curves to define the power produced by the turbine model at various wind velocities [Twidell and Weir, 2015]. Power curves are characterised by cut-in wind speed, when the turbine first starts rotating and producing power; rated wind speed, the minimum speed for which the turbine produces the maximum power output; and cut-off wind speed, when the rotor is brought to a standstill to avoid damage caused by high winds [Twidell and Weir, 2015]. Equation 4.1 describes the power curve in function of the mentioned variables, as calculated

by the EHub [Weimann et al., 2019]:

$$P(v) = \begin{cases} 0 & \text{if } v < v_{in} \\ P_r \cdot \frac{v^3 - v_{in}^3}{v_r^3 - v_{in}^3} & \text{if } v_{in} \leq v < v_r \\ P_r & \text{if } v_r \leq v < v_{out} \\ 0 & \text{if } v \geq v_{out} \end{cases} \tag{3.1}$$

where P indicates the power output, P_r the rated maximum power, v_{in}, v_r and v_{out} represent respectively cut-in, rated and cut-off wind speeds. For the current analysis and the analysis in Part II, three onshore wind turbine models are chosen for new installations. The capacities selected are above 1 MW, because smaller size lose relevance on a national scale. Specifically, they variate between 1.5 and 4.5 MW, which are the upper and lower limits of the sizes installed in the EU-28 in 2017 [Iea Wind,]. The models are chosen from the most diffuse manufacturer and based on availability of the power curves specifications. These are shown in Table 3.1. For simplicity, the reported wind turbines are henceforth referred to as *WT4500*, *WT2500* and *WT1500*. The implementation in the EHub of the non-linear power curve (Eq. 3.1) is tackled by the calculation of the power produced previous to the optimisation process. In fact, the power produced is hourly pre-calculated with wind speed values determined by the TMY. The total power generated for the i-th turbine at the t-th hour is calculated as in Eq. 3.2 [Weimann et al., 2019], with $P_{max,i,t}$ indicating the uncurtailed output for a given wind speed and S_i the integer decision variable representing the number of turbines. So, the power generated is equal of lower than the maximum potential generator at given wind turbine and wind speed; continuous curtailment is applied.

$$P_{out,i,t} \leq P_{max,i,t} S_i \tag{3.2}$$

$$0 \leq S_i \tag{3.3}$$

The investment costs for onshore wind turbine installations are retrieved from [Iea Wind, ,Blanco, 2009] and set at 1100 €/kW for the WT4500, 1250 €/kW for the WT2500 and 1400 €/kW for the WT1500.

3.2 Analysis on the influence of wind speed profiles to the optimal deployment of wind turbines

An analysis is conducted to define to what extent does the selection of wind speed profiles influence the optimal design generated by the EHub. The Drenthe electricity demand shall be supplied either by existing and new wind turbines, or by importing electricity. The cost of electricity imported is set at 10^6 €/kWh, so that the objective costs minimisation ensures a maximisation of the power produced by the wind mills. The analysis is performed by inputting the following wind speed profiles throughout the year:

1. $\overline{v}$: mean wind speed;

Table 3.1: Onshore wind turbines models and technical specifications [turbine models.com, ,Siemens, b].

Wind turbine models	P_r $[kW]$	v_{in} $[m/s]$	v_r $[m/s]$	v_{out} $[m/s]$
Vestas V120-4.5	4500	4	12	25
Siemens SWT2.5-120	2500	3	11.5	22
Vestas V63-1.5	1500	4	16	25

Table 3.2: Amounts of wind turbines deployed by applying 3 wind profiles in the 2σ range.

WT installed [#]	Wind speed profiles $\overline{v}-\sigma$	$\overline{v}$	$\overline{v}+\sigma$
WT4500	0	790	790
WT2500	790	0	0
WT900	0	0	0
WTexisting	9	9	9

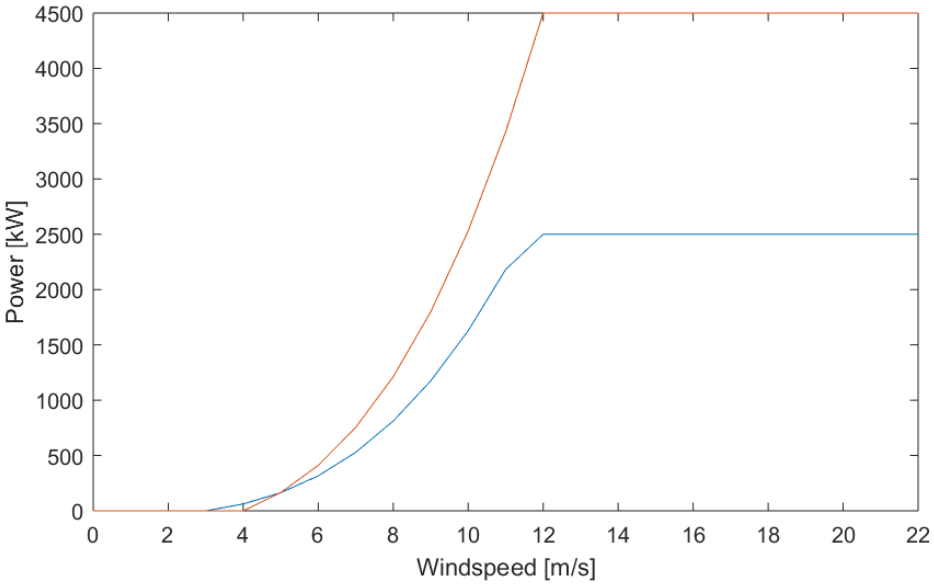

Figure 3.3: Comparison of WT4500 and WT2500 power curves.

2. $\overline{v}+\sigma$: mean wind speed plus one standard deviation;

3. $\overline{v}-\sigma$: mean wind speed minus one standard deviation.

The wind profile database reports wind speeds at a height of 10 m. The EHub calculates the resulting wind speed for an average hub height of 123 m [Twidell and Weir, 2015]. The results obtained from the optimisation are shown in Table 3.2. With the first and second profiles, the optimal design consists of 9 existing wind turbines and 790 WT4500. Whereas, with the third profile WT2500 are installed by the same amount.

The reason of the variation in wind turbine deployment lies in Figure 3.3, which shows the power curves of WT4500 and WT2500 constructed with Equation 3.1. Wind speed values of $\overline{v}-\sigma$ variate between 0.4 and 4.2 m/s and, as Figure 3.3 shows, within values of 3 and 5 m/s the WT2500 produces more power than the WT4500; accordingly, a technology deplyment that ensure an overall larger annual power production is design, with lower electricity imports. It can be said that the optimal design of the system can comprehensively change just taking into consideration wind speeds in the probability range of 68%. Therefore, the choice of representative wind speed profiles influence the design and operation of wind turbines, by means of choosing the wind turbine model whose power curve better catches the range of wind speed. Following, three approaches to overcome the issue and generate a representative meteorological year from the long-term database are presented. The first and last trimester of the year will henceforth be referred to as *winter season*, while second and third as *summer season*.

Chapter 4

Methodology for the generation of a typical meteorological year

4.1 RD Representative days

One of the approaches chosen for generating a TMY is the method proposed by Zang *et al.* [Zang et al., 2012]. It is one of the most widely used methods to generate 12 typical months from a multiple year database [Zang et al., 2012]. For the current research, it is modified for the application of hourly data to select the most representative 365 days out of the multiple years database, to be combined in the generation of one representative year. First, for each day d of the year, the cumulative distribution function (CDF) is calculated in terms of short-term and long-term CDF. Hence, the former is calculated with data of day d for a specific year y, while the latter include data of day d for all the years. Secondly, the Finkelstein-Schafer (FS) comparison statistics [Finkelstein and Schafer, 1971] are calculated as:

$$FS(y,d) = \frac{1}{N}\sum_{i=1}^{N} |CDF_d(v_i) - CDF_{d,y}(v_i)| \tag{4.1}$$

where N indicates the number of readings per day; CDF_d represents the long-term CDF and CDF_d, y the short-term CDF; v_i is the wind speed, discretised in 25 ranges i between 0 and 25 m/s. Five candidate years are selected for better representing day d, by means of lowest FS calculated. Next, the final selection between the candidate years is defined by the lowest root mean square difference (RMSD):

$$RMSD(y,d) = [\frac{\sum_{i=1}^{N}(v_{d,y,i} - \overline{v}_d)^2}{N}]^{\frac{1}{2}} \tag{4.2}$$

Where $v_{d,y,i}$ is the wind speed data of day d, year y and hour i and $\overline{v}_d$ is the mean wind speed for day d, calculated taking into account the whole database. Finally, for each day d, a representative day is selected with low FS and minimum $RMSD$, generating a representative year.

4.2 EP Expected profile

The second method proposed for generation of a TMY employs the long term database to define the mathematical expectation of the profile. The expected value of wind speed is computed from the probability distribution of the individual hour, by summing the values the variable can assume, multiplied

by the probability for the value to occur [Madow, 1968]. The probability is here defined as Weighting Factor WF and the expected value of wind speed $v_{expected}$ is calculated as:

$$v_{expected} = \sum_{i=1}^{25} v_i \cdot WF(v_i) = \sum_{i=1}^{25} v_i \cdot \frac{f(v_i)}{\sum_{i=1}^{25} f(v_i)} \tag{4.3}$$

where v_i corresponds to the 25 ranges introduced with the discretisation of the variable wind speed and f their frequency. The expected value method has been tested to define an optimal wind turbine, that maximises the annual power produced via the expected wind profile.

4.2.1 Testing the expected wind speed profiles on wind turbine optimisation

The constrained optimisation performed is characterised by the following objective function, which maximises the total expected power produced over the year:

$$\max_{P_r, v_{in}, v_r} \sum_{t=1}^{8760} \sum_{i=1}^{25} P(v_i) \cdot WF(v_{t,i}) \tag{4.4}$$

where $P(v_i)$ indicates the power produced at the i-th range of wind speed, calculated from the power curve function of Equation 3.1. $WF(v_{t,i})$ represents the weighting factor of the i-th range at hour t, as shown in Equation 4.3. The decision variables are P_r, the wind turbine maximum capacity; v_{in}, the cut-in wind speed and v_r, the rated wind speed. These are constrained by a lower and upper limit, as shown in Table 4.1. Furthermore, the results are presented in relation to the available wind turbines; as percentage variation of the annual power produced compared to the maximum produced through the calculated optimal wind turbine.

The results are as expected; the optimal wind turbine has both cut-in and rated wind speed approximately equivalent to the lower limits defined, in line with current trends of wind turbine development. In fact, the technology is directed not only towards larger capacities and hub height, but also longer blades. Through the advancement of lighter materials and improved design, the weight of the blade increases unproportionally to its volume [Junginger, 2005]. Hence, the wind required to win the rotor inertia tends to decrease with later designs; decreasing the cut-in and rated wind speed and increasing the annual power produced, at equal capacity and wind profile. Current wind turbines models have cut-in wind speeds in the range between 3 and 4 m/s, and rated wind speed between 10 and 15 m/s [turbine models.com,]. The results show that even the best available turbine, the WT4500, produces less than half of the annual power compared to the optimal wind turbine; and the worst has a production almost 10 times less than the optimal, due to the high rated wind speed and relatively high cut-in. It is also important to notice that the wind turbine models chosen do not correspond to the most recent models commercialised, as the specification of these are not found.

Table 4.1: Constraints and results of optimisation problem.

	P_r $[kW]$	v_{in} $[m/s]$	v_r $[m/s]$	P_{annual} $[kWh]$	Variation [%]
Lower bound	1500	2.0	10.0		
Upper bound	4500	5.0	16.0		
WT optimal	4500	2.1	10.0	5.95e+06	
WT4500	4500	4.0	12.0	3.13e+06	-47
WT2500	2500	3.0	11.5	2.18e+06	-63
WT1500	1500	4.0	16.0	4.63e+05	-92

4.3 ES Expected Spikes

Both the profile modelling methods described so far do not properly account for wind speed spikes. However, these acquire importance if storage is displaced, because their exclusion may cause an underestimation of the appropriate storage capacity to install. The following section describes how real wind speed peaks are taken into account to integrate the previously calculated *expected profiles* with *expected spikes*. First, a definition of wind *spike* is set and then a statistical analysis of amplitude and frequency of the spikes allows the computation of expected positive and negative peaks to be added to the expected profile calculated in section 4.2.

Figure 4.1 illustrates the distribution of wind speed, from the first to the 100th hour of the year. The expected profile runs along the *Time* dimension, with the expected value corresponding to the database mean for hour t. It is set that the top 5% highest wind speeds over the whole database are treated as spike. The black line in Figure 4.1 is the threshold wind velocity determining the spike, calculated as 9.3 m/s. The positive spikes are further analysed in the context of their probability distribution, to define the expectation for a certain amplitude to occur. At the same time, the amount of peak events are recorded to define the frequency of the expected spike.

The probability distribution of the amplitude and frequency of spikes may consistently vary depending on of the season of the year or the time of the day. So, the distributions are determined for various periods. For the current analysis, the number of periods is set at 4. Figure 4.2 show the probability distribution of the positive spike amplitude and frequency for the first and second trimesters of the year. From January to March the expected number of spikes are 183 and their amplitude reaches a value of 22

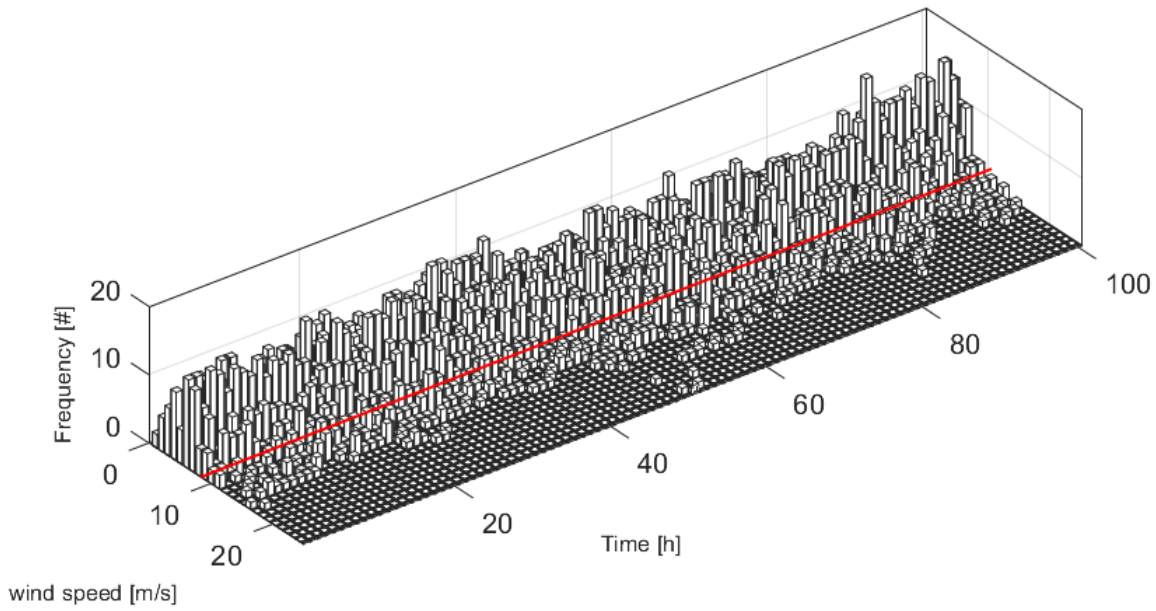

Figure 4.1: Frequency distribution of wind speed data from 1951 to 2017, from hour 1 to hour 100 of the year.

m/s. From April to June on the other hans, 48 spikes are expected with a maximum amplitude below 18 m/s. The spikes are then randomly integrated to the *expected profiles*, for an amount corresponding to the expected frequency and amplitudes randomly selected from their probability distribution.

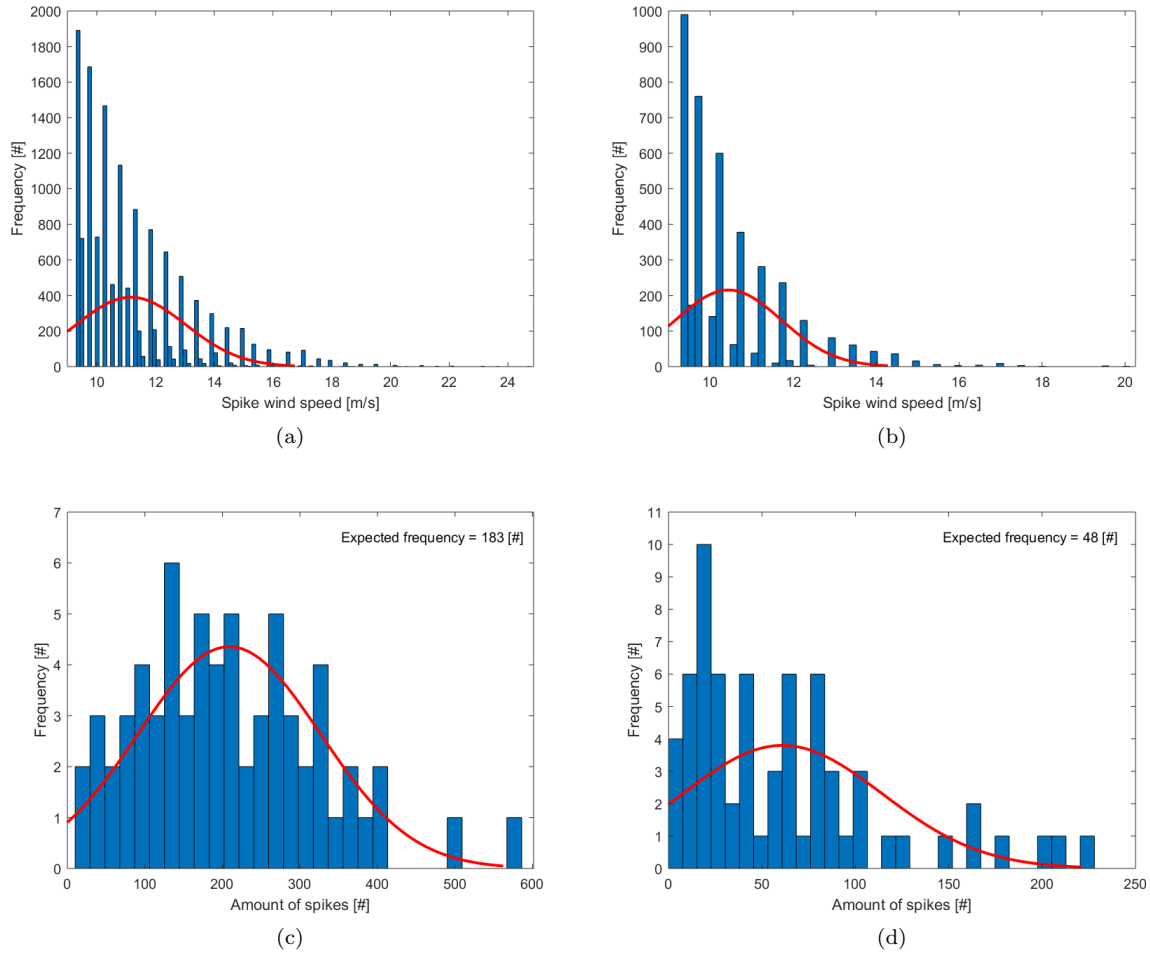

Figure 4.2: Histogram defining the amplitudes probability distribution in the first (a) and second (b) trimester of the year, and the amounts of spikes occurred in the first (c) and second (d) trimesters.

The same approach is applied to the negative peaks. The threshold wind velocity is set at 3 m/s, corresponding to the lower limit at which none of the wind turbines models selected produces power. Therefore, the negative peaks consist of the number of hours at which the wind turbines produce no power.

Chapter 5

Results

The TMY of wind speed profiles calculated with the RD, EP and ES methods are here displayed and commented, together with real yearly profiles used for comparison. Figure 5.1 reports real wind speed profiles of four randomly selected years from the database. Real data presents large variations throughout the year, reaching peaks of over 20 m/s during winter season. Figure 5.2 shows the wind profile calculated with the RD method. Although the values present reasonable fluctuations and higher velocities during winter time, both the positive and negative peaks are consistently limited in comparison to real data. In fact, the maximum positive peak reported is about 13 m/s, whereas for real data this reaches 20 m/s. On the other hand, the EP profile ranges between 3 and 8 m/s (Figure 5.3), disregarding both positive and negative spikes, as shown in Figure 5.3. As previously stated, the expected value of the probability distribution corresponds to the average value of the database; consequently, the positive and negative spikes are outweighted by the variability previously shown in Figure 3.1 and 3.2. Figure 5.3 also shows a larger variation of wind speeds expected during the summer season, when higher variability of daily/nightly wind speed is expected; whilst smaller variation but higher values are expected during winter season. It can be said that the offset of extreme wind speed performed by the EP method, both positive and negative, hinder the main problem of unpredictable weather, that is intermittency. Finally, the wind speed profiles with the inclusion of expected spikes is displayed in Figure 5.4. The latter records wind peaks up to 20 m/s, with higher frequencies expected at winter time. The graph also shows a considerable number of negative peaks along the whole year, slightly more dense during summer time. On the one hand, ES reports accurate magnitude of spikes; on the other hand, the length of the episode is not taken into consideration and consecutive hours may drastically variate. For instance, a positive and negative peak could be consecutive, creating an unrealistic sequence. Hence, the quality of steady offshore winter wind speeds may be totally disregarded. Instead, the RD method is able to better catch real sequences of wind speed of the length of 24 hours, as a result of its construction method.

The results are further tested by applying them to the Dutch case-study; the electricity grid is optimised with a cost minimisation approach and operation of NDRES are analysed with the three methods of TMY. Part II of the research describe first, a modest improvement on the Ehub framework in regard of installation costs for offshore wind parks; secondly, the overall system analysed is described and results for the various weather profiles are shown.

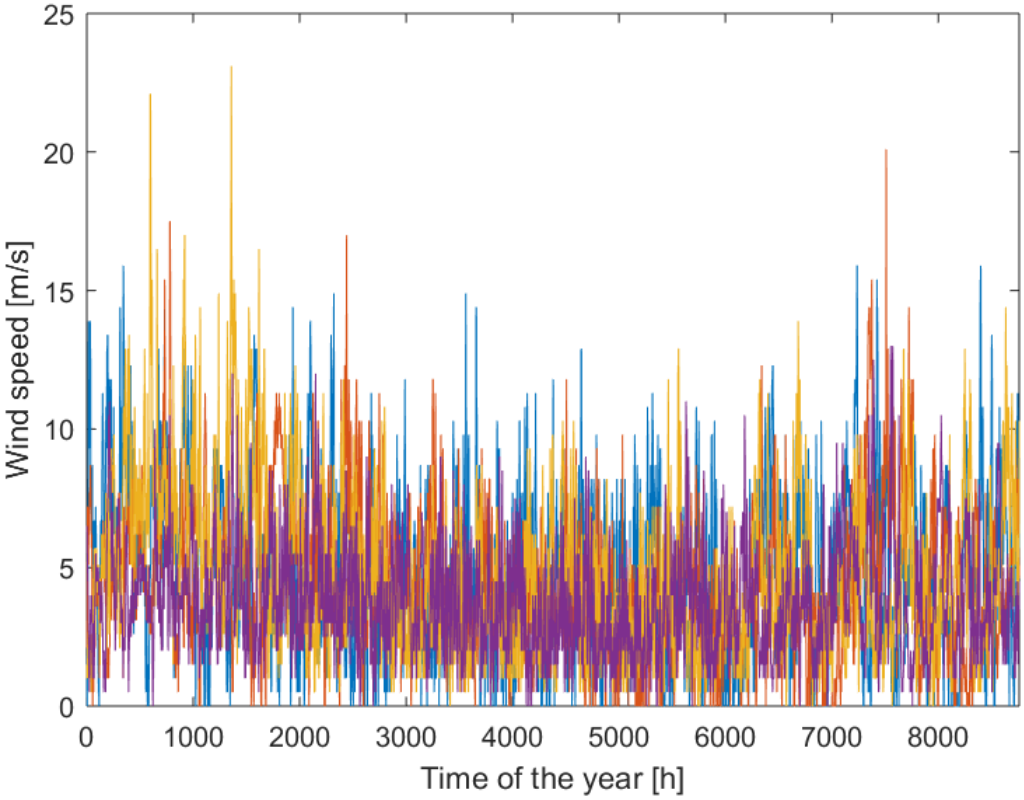

Figure 5.1: Real wind speed profiles of four randomly selected years between 1951 and 2017.

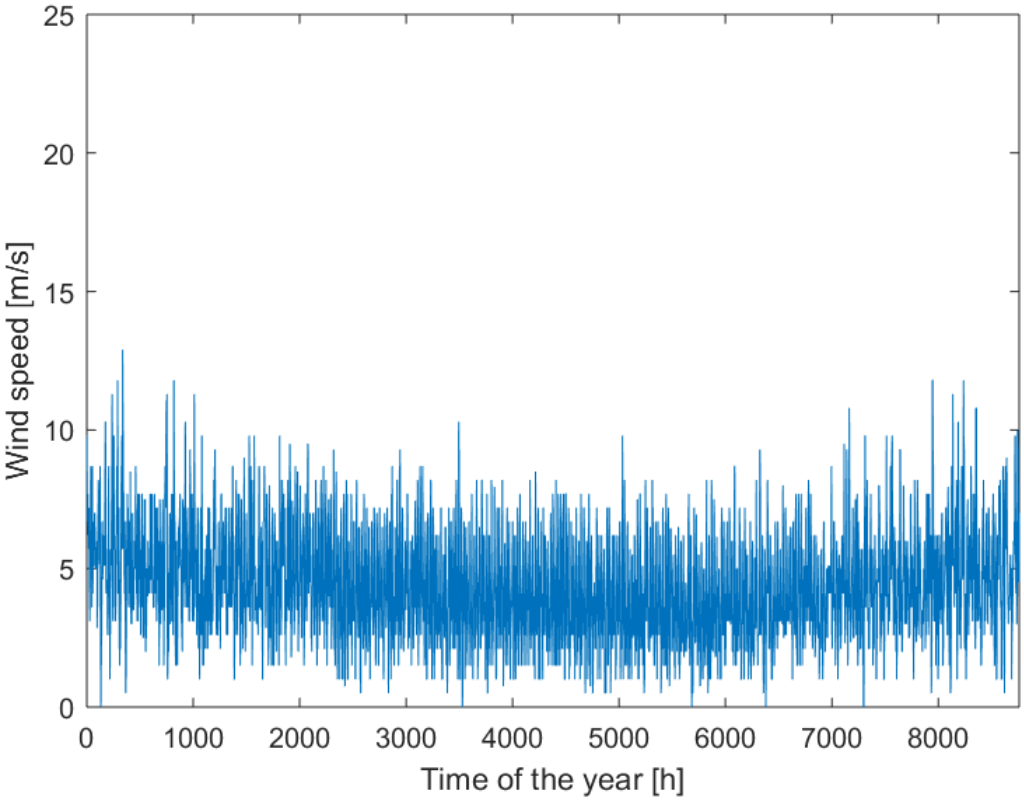

Figure 5.2: Wind profile calculated with the method of RD.

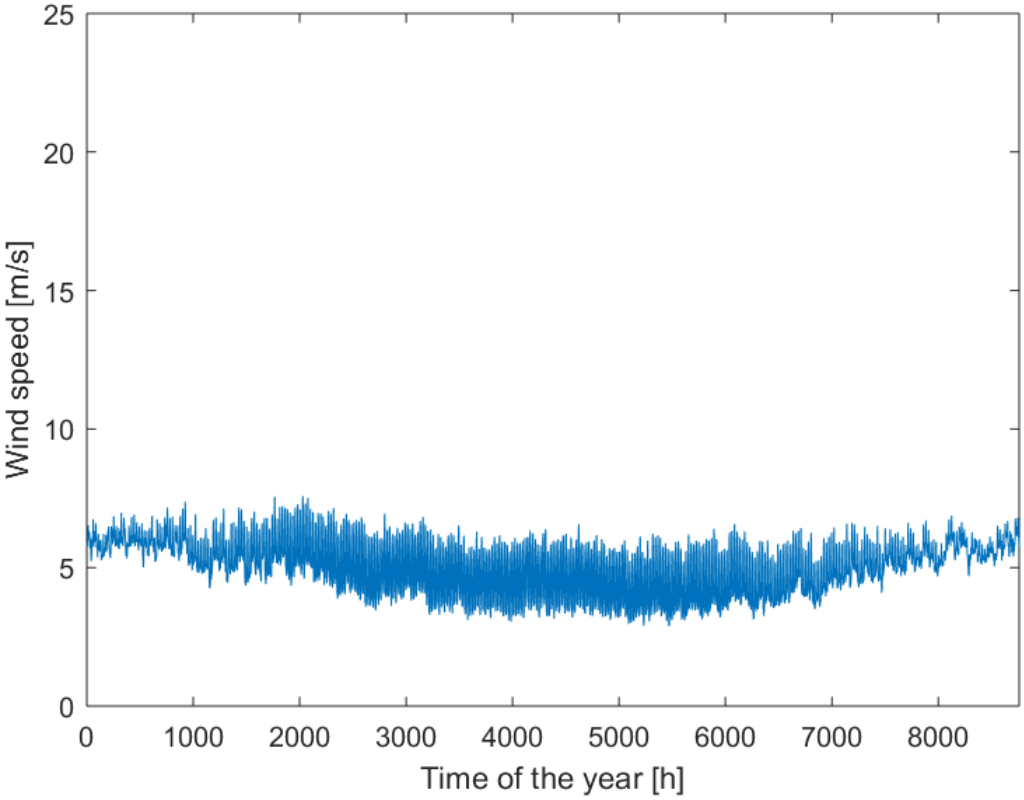

Figure 5.3: Wind profile calculated with the EP method.

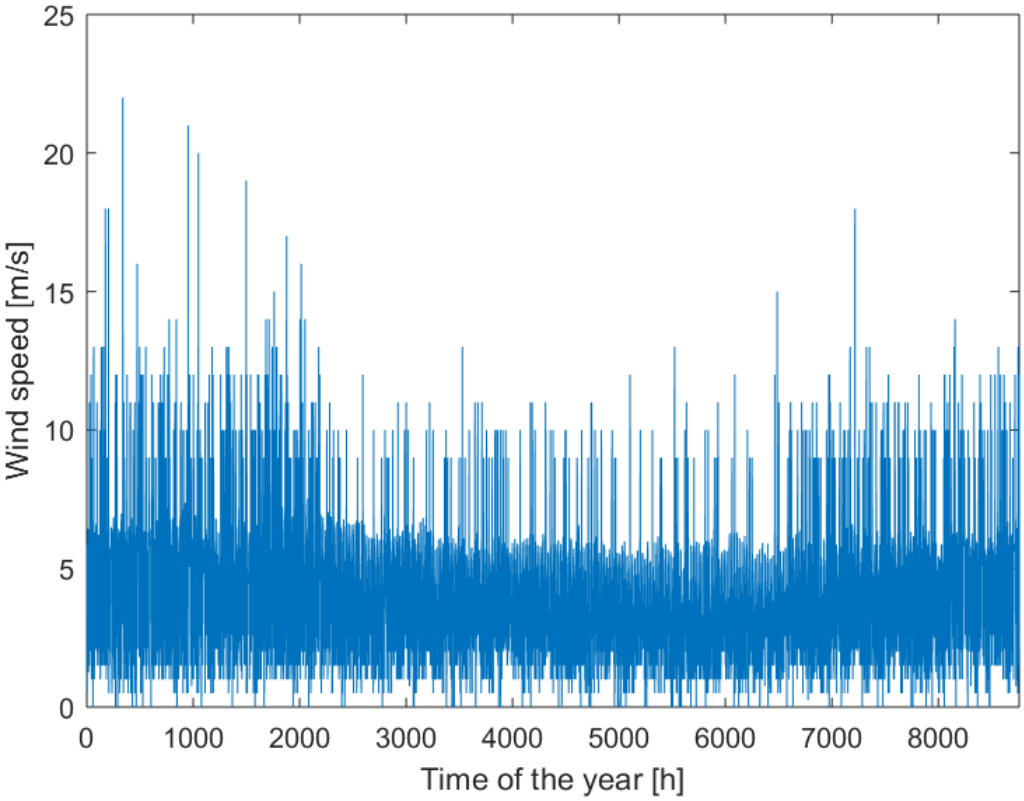

Figure 5.4: Wind profile calculated with ES method, for 4 periods of the year.

Part II

Case-study: the Dutch electricity grid

Chapter 6

Modelling of offshore wind turbines investment costs

In recent years, offshore wind turbine installations have been growing faster than the onshore counterpart. In fact, offshore wind parks are subjected to more favorable wind speeds, together with minor limitations given by space constraints and public acceptance [Junginger, 2005]. However, investment costs for offshore applications are approximately 50% higher than onshore ones due to complex construction, installation, foundations and grid connection [Bilgili et al., 2011]. Whilst onshore investment costs are currently well known and dominated by wind turbine costs, the offshore counterpart strongly depends on the conditions of installation, rising with water depth and distance from shore [Junginger, 2005]. As a matter of fact, foundation and grid connection constitute up to 70% of the total investment costs [Junginger, 2005]. Currently, technological learning for offshore wind farms is object of study [Wiser et al., 2016, Van der Zwaan et al., 2012]. Cost diminishing is not noticeable; one of the issues derives from the locations of new installations. In fact, since earlier projects, water depths have doubled and shore distances tripled [Voormolen et al., 2016], with installation costs rising accordingly. Furthermore, raw material costs have increased due the rise in commodity prices over the last decade, for instance steel and copper [Voormolen et al., 2016].

In the context of high uncertainty on the appropriate investment costs, data for this research is based on a European Environment Agency report from 2009 [European Environmental Agency, 2009], the focus of which lies on the cost increase depending on water depth and distance from shore in the North Sea. The data provided refers to a baseline 200 MW wind farm using 2 MW turbines, 5 km from shore in water depth of 15 m [European Environmental Agency, 2009], whose investment cost is 1800 €/kW. The cost variation is provided for four ranges of water depth and eight ranges of distance from shore. First, the data available is categorised between wind turbine costs, regardless of location (772 €/kW), and installation costs (1028 €/kW, including foundation, grid connection, etc.). The latter are plotted in Figure 6.1, where distance from shore is the average of the corresponding range bounds. Then, a linear interpolation is performed for data of the same water depth. Four linear equations are obtained for installation costs IC, one for each water depth range WD and function of distance from shore DS. The equations applied in the EHub to define the offshore installation cost are as follows:

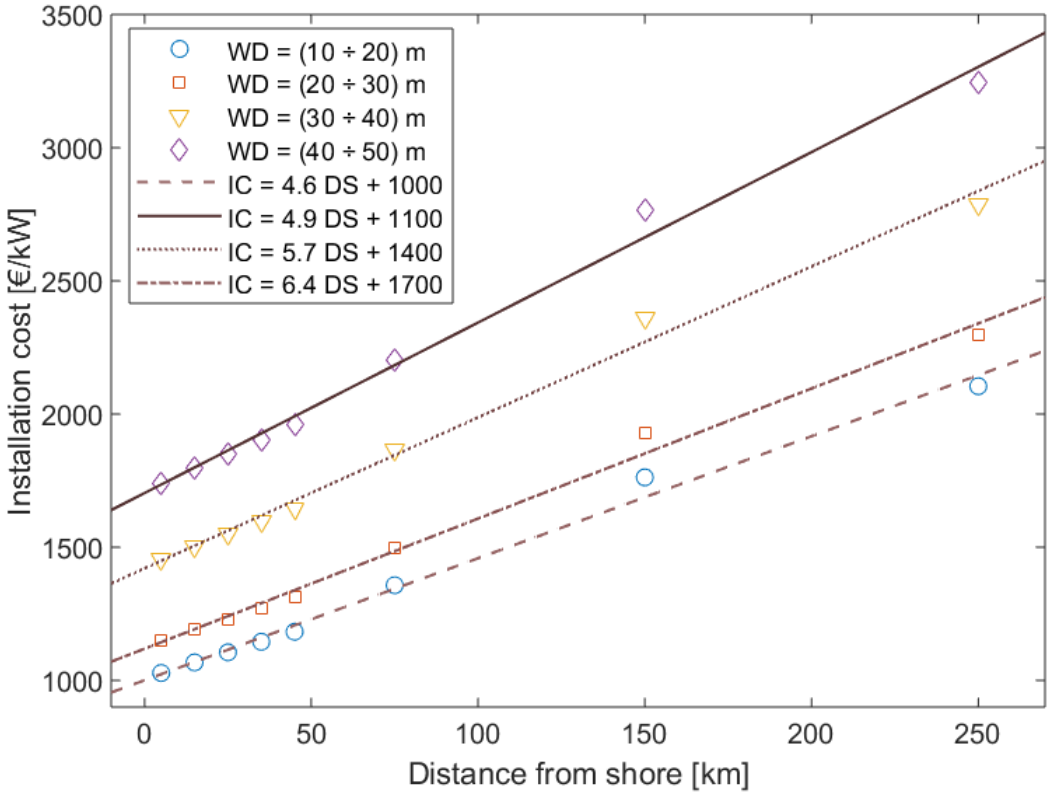

Figure 6.1: Offshore investment cost data and linear interpolation to define the cost depending on distance from shore, for four ranges of water depth [European Environmental Agency, 2009].

$$IC(WD, DS) = \begin{cases} 4.6 \cdot DS + 1000 & \text{if } 10 \leq WD < 20 \\ 4.9 \cdot DS + 1100 & \text{if } 20 \leq WD < 30 \\ 5.7 \cdot DS + 1400 & \text{if } 30 \leq WD < 40 \\ 6.4 \cdot DS + 1700 & \text{if } 40 \leq WD < 50 \end{cases} \tag{6.1}$$

To conclude, it must be noted that the offshore wind turbine capacities, included in the second part of this study, are between three and five time larger than the turbines examined by [European Environmental Agency, 2009], so the baseline cost of 1800 €/kW could significantly decrease due to economy of scale. However, the investment costs are maintained as in [European Environmental Agency, 2009] due to various factors: the rise of wind turbine capacity increases the foundation cost because of hte increase in weight to support [European Environmental Agency, 2009]; the increase of commodity prices over the last decades is not recorded in the 2009 report; also, for lack of better data available and time constraint on the research.

Chapter 7

Methodology for Dutch case-study

The following chapter provides a description of the energy system investigated to determine the optimal design and operation of the Dutch electricity grid with NDRES coupled with large-scale hydrogen storage. The optimisation is performed with a cost minimisation approach. The electricity grid is emulated through multiple energy hubs, whose goal is to supply electricity to the Dutch consumers. The inputs to provide to the EHub are the following: hourly weather profiles throughout the TMY, hourly electricity load, modality of distribution, type of decentralised energy hubs and their interaction, technology costs and technical specifications, as well as technical potential for various types of installation.

First, the MES under study and the technologies adopted are described and then the chapter reports the decentralisation methodologies, together with a characterisation of the various types of energy hubs adopted and the network. Methods for data gathering and analysis are also reported.

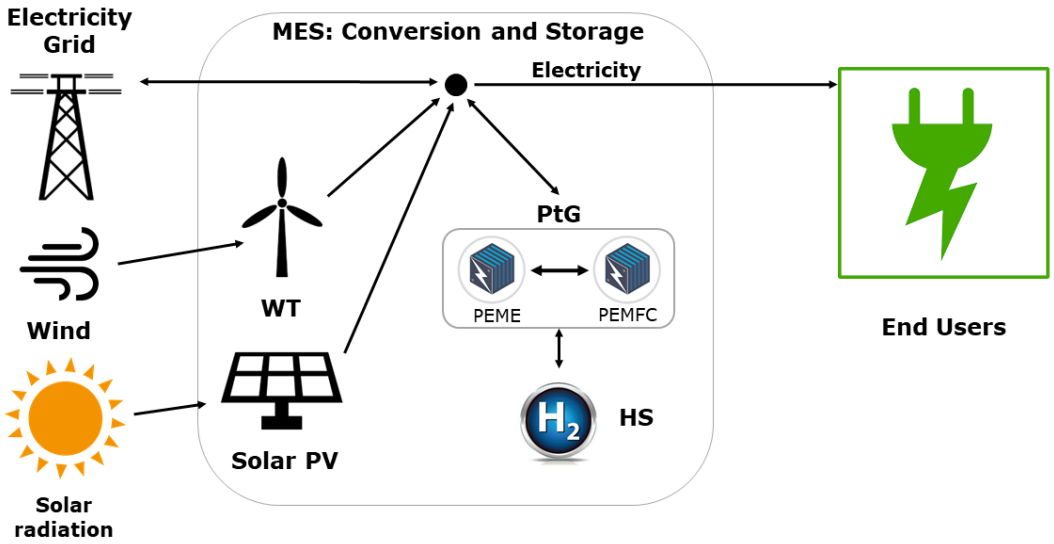

Figure 7.1: Schematic representation of the multi-energy system analysed.

7.1 MES

An integrated MES is schematically represented in Figure 7.1. The end users shall be supplied with electricity generated by wind turbines, solar PV and Proton Exchange Membrane Fuel Cell (PEMFC) fed by hydrogen, or by importing electricity through the grid. A brief description of the technologies adopted follows.

7.1.1 Wind Turbines

Wind turbine technology is described in Chapter 4; however, further information is given about existing and newly installed offshore wind turbines.

Offshore wind turbines

Onshore and offshore wind turbines differ in various aspects; offshore wind turbine models must be more reliable and resistant to corrosion compared to the onshore counterpart, due to salinity exposure and higher maintenance costs. Additionally, larger capacities allow greater generation with more favorable offshore wind speeds, which are higher and steadier [Kaldellis et al., 2016].

Two models are selected for offshore installations, shown in Table 7.1. The Vestas V164-9.5MW turbine ($WT9500$) is the largest turbine whose technical specifications could be retrieved; also, its utilisation is planned for the *Borssele V* wind farm [MHI Vestas Offshore,], one of the wind farms to be built by 2030. The Siemens SWT-6.0-120 wind turbine ($WT6000$) is selected for smaller offshore installation. The reported selection intends to reflect the technical direction towards larger capacities, in view of the copious future offshore installations. Table 7.1 also reports model specifications. The constraint on the number of possible turbine installation is calculated as for onshore, with a radius of 500 m around each tower. The sea availability has been set equal to the area delimited by the Government for installation up to 2030, for a total of 2900 km^2 [The Ministry of Infrastructure and the Environment, 2014].

Existing wind turbines

The existing wind turbines on Dutch land and sea, with capacity higher than 1 MW, have been retrieved from [Windstats,] and embodied in the EHub. They consist of 43 models accounting for about 78% of existing Dutch wind turbines. They contribute to the total maintenance expenses but not to investment costs. The number of wind turbines models to include in the EHub determines an overall increase in binary variables, hence a rise in computational complexity. However, their inclusion consents to determine whether and when existing farms should be replaced. Weimann *et al.* [Weimann et al., 2019] reports the method applied to integrate existing wind turbines in the EHub, with particular focus on the generation of their power curves.

7.1.2 Solar photovoltaic

Solar PV installations have grown exponentially since about 2000. Earlier, they were manly used for stand-alone applications, while grid-connected PV has currently become the main utilisation, either

Table 7.1: Offshore wind turbines models and technical specifications [MHI, ,Siemens, a].

Wind turbine models	P_r $[kW]$	v_{in} $[m/s]$	v_r $[m/s]$	v_{out} $[m/s]$
Vestas V164-9.5	9500	4	13	25
Siemens SWT-6.0-120	6000	4	13	25

incorporated in buildings or as large free-standing arrays. Solar PV cells are constituted by one or two layers of semiconducting materials, usually silicon. The photons of electromagnetic radiation on the PV cell creates an electric field across the layers, causing electrons to flow and generating power [Twidell and Weir, 2015]. The current research includes solar PV installation on buildings, so the technical potential for installations depends on the Dutch rooftop space available. The generated electrical power from PV is calculated by the EHub as [Gabrielli et al., 2018]:

$$P_t < \eta(I_t, \Theta_t) I_t S \tag{7.1}$$

where P is the power generated as the t-th hour, η is the conversion efficiency, function of solar radiation I and air temperature Θ; S represents the installed PV area, limited by space constraint. Eq. 7.1 implies continuous curtailment, as applied to power generation from wind turbines. Defaix *et al.* [Defaix et al., 2012] calculates the technical potential for PV installation on buildings in the EU-28 context; 200 km^2 are found available for the Netherlands. To conclude, investment costs for solar PV installations are set at 200 €/m^2, based on [Van Sark, W.G.J.H.M.; Schoen, 2016, SolarSolutions, 2018], both focusing on Dutch market prices.

7.1.3 PtG: PEM fuel cell, PEM electrolyser and salt cavern hydrogen storage

The possibility of using excess power to create hydrogen has recently gained interest; in fact, hydrogen is versatile for various energy sectors [Barbir, 2009]. In the context of this research, PtG refers to the production and re-conversion of hydrogen, by means of a three-stage process. Following, a brief description of the phases are reported. [Gabrielli et al., 2018] and [Poluzzi, 2017] report details about PtG modelling, together with technical and economic specifications applied in the EHub.

Proton Exchange Membrane Electrolyser (PEME)

The electricity generated by NDRES, and not instantly consumed by the users, may be used for the water splitting process performed by PEME; the electrolyser uses energy for driving the endothermic reaction of hydrogen and oxygen disassociation, as follows:

$$H_2O \rightarrow H_2 + \frac{1}{2}O_2 \tag{7.2}$$

H_2 storage in salt caverns

Subsequently, the high pressure hydrogen produced by PEME is injected underground. Salt caverns are selected for the application as they benefit from the following advantages over other geological storage solutions: the saline environment prevents the onset of chemical reaction which can consume the stored hydrogen; high withdrawal and injection rates; storage volume provided is acceptable, with reasonable costs; Furthermore, salt caverns ensure the high pressure storage conditions required from hydrogen [Poluzzi, 2017].

Proton Exchange Membrane Fuel Cell (PEMFC)

PEMFC is the electricity generator of the PtG system, fed with the clean fuel hydrogen. Fuel cell technology has the advantage of erasing the limitation of the Carnot efficiency, typical of heat engines, reaching efficiencies of 80% [Salameh and Salameh, 2014]. In fact, the combustion phase is avoided by converting isothermally chemical energy to electric energy [Cengel and Boles, 2015]. The PEMFC produces electricity electrochemically, employing hydrogen and air. A PEMFC is composed of

two electrodes, anode and cathode, separated by an electrolyte, a proton conducting polymer. Initially, the fuel is ionised on the surface of the anode, then the ions flow to the cathode from the electrolyte. Following, the chemical reaction on the Anode and Cathode, in order:

$$H_2 \rightarrow 2e^- + 2H^+ \tag{7.3}$$

$$2e^- + 2H^+ + \frac{1}{2}O_2 \rightarrow H_2O \tag{7.4}$$

The potential difference created between anode and cathode allows free electrons to flow through an external circuit, generating electricity. The hydrogen ions react with oxygen to form water, by-product of the process together with waste heat released from the exothermic reaction [Cengel and Boles, 2015].

7.2 Geographical discretisation - 28 nodes

The technologies composing the MES are explained. In the forthcoming section, the hubs positioning is described. The Electricity demand and generation is decentralised over multiple energy hubs, the *nodes*. The 12 Dutch provinces are represented by Province Nodes (PN), the offshore wind farms by four Offshore Nodes (OSN) and the other 12 nodes represent the locations of Salt Caverns, where hydrogen can be stored (SCN). Figure 7.2 shows the location of the nodes on the territory, where the yellow dots are the PN, the red dots are the OSN and the pale blue ones the SCN.

7.2.1 Province nodes

The delivery of the PN hourly electricity demand is the first objective of the Ehub. In loco power production is available through onshore wind turbines, existing or new, or by rooftop solar PV, both reliant on weather conditions. The weather database for this type of node includes wind speed and solar radiation profiles. For each PN, the database is constructed based on the weather station data as listed in Appendix A, to define the average value at a specific year and hour. A database is also created for air temperature, which has influence on solar PV and fuel cell performances; however, this is a unique database employed independently from decentralisation. The databases are applied for the generation of the TMY with the methods described in Chapter 4. The installations of wind turbines in the PN are constrained by area availability. The technical potential of installation is assumed to be limited to 15% of the total land [McKenna et al., 2015, The World Bank,], as reported in Appendix B. Regarding technical potential for PV installations, the value retrieved of the total Dutch rooftop area available is allocated over the PN in proportion to the built-up area [Centraal Bureau voor de Statistiek,].

Electricity demand

The total electricity demand of the Netherlands for 2017 has been retrieved from [dem,]. To appropriately allocate the demand over the provinces, first of all, the load is separated into electricity consumed by the residential sector and by the industrial sector [Centraal Bureau voor de Statistiek,]. The residential electricity demand is then allocated on the basis of density of population, while the industrial electricity consumption is allocated based on the concentration of energy-intensive industries

(EEI)[1] located in any one province. The electricity demand for PN results from:

$$E^P_{total} = K^P_{population} \cdot E^{NL}_{residential} + K^P_{industry} \cdot E^{NL}_{industrial} \tag{7.5}$$

$$K^P_{population} = \frac{population^P}{population^{NL}} \tag{7.6}$$

$$K^P_{industry} = \frac{EEI^P[\#]}{EEI^{NL}[\#]} \tag{7.7}$$

where E indicates the electricity consumption, its subscript refers to a sectoral allocation whilst the superscript to a spacial distribution; K is the index used for allocating the demand over population or industry. The results are presented in Appendix B.

7.2.2 Offshore nodes

Four OSN are designated, each one of them representing a portion of sea delineated by the government for offshore wind turbine installations by 2030 [The Ministry of Infrastructure and the Environment, 2014]. Their surface delimitation determines the maximum technical potential for new or existing[2] offshore wind turbines. Various weather stations are located in the North Sea [KNMI, a]; databases for each OSN are created by the stations closely surrounding the node. An average of the historical records is performed, weighted over distance of the weather stations from the node, as reported in Appendix A.

Wind turbine installation costs differ for each OSN, because of their dependency on water depth and distance from shore. They are calculated based on the analysis performed in Chapter 3. The average water depth and distance from shore of the node is retrieved from [te Raa et al., 2010], and the installation costs calculated as in Eq. 6.1. Table 7.2 shows the results obtained.

7.2.3 Salt cavern nodes

Twelve SCN are designated for the storage of hydrogen. The selection is carried out on the basis of suitable geological formation on the Dutch territory. TNO reports the location of suitable caverns for the type of construction required with a height of 300 m [TNO,]. These nodes are exclusively used for storage purposes or power production from hydrogen. PtG is the only technology applicable in SCN.

The Dutch case-study with a 28-nodes discretisation is not resolved for this research, because the result is a non-solvable problem for reasons explained by [Weimann et al., 2019].

[1] for the current analysis the following have been included: steel, iron, cement, paper, chemical and petrochemical industries [EuroPages,].

[2] Gemini, Prises Amalia, Egmond aan Zee, Luchterduinen [4C,].

Table 7.2: Offshore nodes for the Dutch case-study and the installation cost of wind turbines in dependence of water depth and shore distance, relatively to a baseline cost of 1028 €/kW, for a 200 MW wind farm composed by 2 MW turbines, at water depth 15 m and 5 km distant from shore.

OS Nodes	Avg. water depth $[m]$	Avg. shore distance $[km]$	Installation cost [€/kW]
North Wadden Island	30 - 40	80	1856
Holland Coast	20 - 30	35	1272
Borssele	30 - 40	50	1685
IJmuiden Ver	20 - 30	75	1468

Figure 7.2: Dutch map representing type and location of decentralised system with 28 nodes.

7.3 Geographical discretisation - 3 nodes

For the aforementioned reason, additional simulations are carried out with 3 nodes to decrease the computational complexity. The three categories of nodes described in the previous section are now represented by one node, with same features of the previous multiple-nodes. The *Onshore* node is characterised by technical potential for wind turbine and solar PV installations equal to the sum of the PN area constraints. The *Offshore* node is a fictitious portion of sea of 2900 km2 with water depth and distance form shore averaged over the previous nodes. Both the described nodes include the existing Dutch wind turbines with a capacity equal to or greater than 1 MW, onshore or offshore. The weather database is created using data retrieved from a limited number of weather stations distributed all over the country, with records from 1951. The *SCavern* node is employed for the installation of PtG systems with storage of hydrogen carrier.

The 3-nodes case study is also applied for a sensitivity analysis, to define the effect of increasing the technical potential constraint for offshore wind turbine installations on design and operation.

7.4 Electricity grid

To conclude, the following section describes node interaction with the electricity grid. Two carriers are included in the analysis; electricity and hydrogen. However, only electricity is installed as network for the current research. In fact, it is assumed that a hydrogen network would not be implemented because it is more expensive than the electricity grid, which is free of charge for the EHub. The type of interaction between nodes used for the simulations is defined as *Grid*, whose modelling differs from the *Network* option, this will not be discussed further here. The *Grid* option allows the definition of whether each node shall, should not or could be connected to the grid, without considering the direct connection between nodes. The energy balance on grid level offsets the flows entering and leaving the linked nodes, as well as electricity imports and exports, calculated as follows for each hour of the year:

$$\sum_{i=1}^{N}(flow_i - import_i + export_i) = 0 \tag{7.8}$$

where N indicates the total number of nodes i. The flows are expected to be directed towards the PN, or *onshore* node, where the electricity load is concentrated. They shall receive electricity flow instantly, produced by the OSN, or *offshore* node, or by the stored energy in the SCN, or *SCavern* nodes. Additionally, an energy balance is applied on the nodes:

$$production_i + flow_i + violation_i - dissipation_i - demand_i = 0 \tag{7.9}$$

where *production* of the i-th node indicates the generation in loco, the $flow$ represents the electricity entering (positive) or leaving (negative) the node and *demand* is the electricity consumed, greater than zero for the onshore node(s). $Violation$ indicates the non-delivered demand and increases the overall cost by 5000 €/kWh. Instead, *dissipation* indicates the amount of electricity generated but not utilised, with same costs added to the system as violation. A remark shall be made with regards to the *import* and *export* of electricity. Whilst the modelled system physically admits imports and exports from the individual nodes, they are only balances on the overall grid (Eq. 7.8). Therefore, the resulting imports and exports of the nodes are not mathematically relevant, but their sum is to the grid balance. To conclude, the electricity imports represent the only cause of CO_2 emissions of the system analysed. Over 70% of the Dutch electricity imports is delivered by Germany [TenneT, 2018]. Therefore, the import price and specific emissions are fixed to the current German export price of 0.032 €/kW, with an emission factor of 0.676 kg_{CO_2}/kWh based on current fuel mix generation [Kono et al., 2017]. Furthermore, a CO_2 tax of 20 €/kWh is applied.

Chapter 8

Evaluating the impact of various methodologies for TMY

The 28 nodes case-study results unfeasible at this stage. Therefore, results for the 3 nodes discretisation case-study are analysed. Three simulation are conducted for three scenarios; the methods of TMY are applied to wind and solar radiation profiles, used as input of the EHub. Electricity import are not allowed, thus causing violation if the production in loco is not sufficient to satisfy demand. Table 8.1 reports the optimal technology deployment calculated by the EHub, with a cost minimisation approach. The optimal design slightly varies, but the area available is fully employed for installations for all scenarios. The onshore wind turbine installations more than double the offshore counterpart, due to larger constraint. Overall, the most relevant alteration between the three scenarios is the partial maintaining of existing wind turbines, for EP profiles. Figure A.1d in Appendix A shows that offshore wind speed for EP scenario do not rise over 12 m/s, as opposed to RD and ES scenarios. In fact, limited wind speed of EP would not take advantage of the newly larger capacities installed. So, the replacement of existing turbines with potential larger power production is not as relevant for the other scenarios, where all the existing turbines are replaced. The limited wind speeds also cause the smaller size of PEME for EP scenario; overproduction is limited in comparison to the other scenarios due to limited maximum wind speeds, 8 and 12 m/s respectively for onshore and offshore. However, the level of autarky achieved with EP profiles is almost 100%, thanks to the absence of no-wind hours. Figure 8.3c depicts the electricity overproduction entering the PEME for EP scenario; the flow is positive for most of the year, whilst the RD and ES counterparts only report peaks of flow, as shown by Figure 8.3e and 8.3a. Consequently, the amount of energy stored by hydrogen in the salt caverns is in the order of 4.9e+07 for EP (Figure 8.2b) and only half for the RD and ES (Figure 8.2a). Nevertheless, the amount of electricity stored for all scenarios represents only a small percentage of the total demand, in the order of 10^4.

8.1 Electricity production

Although the system design only slightly changes for the three scenarios, the way electricity is generated differs. Onshore wind turbines account for most of the production for RD and ES scenarios, almost reaching half of the load; whilst offshore wind turbines production is more relevant for EP scenario, as shown in Table 8.2. Solar PV, which is installed up to its technical potential in all the scenarios, generates an additional 10% of the demand in the EP scenario. The reasons for variation lay on the input weather profiles, shown in Appendix A, Figure A.1, determining the amount of electricity generated along the year by the various technologies (Figure 8.1). The RD scenario experiences an

Table 8.1: Technology deployment with 3 nodes optimisation; weather profiles calculated with RD, EP and ES method. Wind turbine unit is amount of turbines [#]; solar PV unit is [m^2]; PEME, PEMFC and H2 storage unit is [kW].

		TMY method		
Technologies	Unit	RD	EP	ES
WT1500	#	0	0	0
WT2500	#	0	0	0
WT4500	#	8108	8106	8109
WTex (onshore)	#	40	42	39
WT6000	#	0	0	0
WT9500	#	3692	3633	3692
WTex (offshore)	#	0	59	0
solar PV	m^2	2e+08	2e+08	2e+08
Electrolyser (PEME)	kW	100	75	100
H2 storage	kW	196349	196349	196349
Fuel Cell (PEMFC)	kW	500	500	500

Table 8.2: Level of autarky reached with the three methods for TMY, together with the ratio of demand supplied by NDRES; ratio of annual electricity produced by PEMFC over the demand is reported.

	RD	EP	ES
Autarky	72.5 %	99.9 %	69.5%
WT onshore production	48.0 %	27.9 %	49.6 %
WT offshore production	11.8 %	50.0 %	7.9 %
solar PV production	12.7 %	22.0 %	12.0 %
PEMFC production [$\cdot 10^{-5}$]	8.6 %	21 %	3.9 %

onshore wind power production approximately constant along the year due the small seasonal variation of the wind profile (Figure A.1a); instead, the offshore counterpart has larger seasonal variation but lower overall production, due to the smaller amounts of offshore wind turbine installed and limited hours of wind at stronger conditions than the turbine rated wind speed 13 m/s, which would otherwise allow to fully take advantage of the rated large capacities. The mentioned phenomenon is particularly evident in summer time, when lower wind speeds are overall recorded. The EP scenario is the only one with offshore wind power production more relevant than onshore counterpart, especially in the season with lower wind. Figure A.1d shows that, although offshore wind speed for EP scenario do not rise over 12 m/s, offshore production is relatively consistent all year long thanks to the absence of wind speeds below 5 m/s, allowing the offshore farms to consistently send to shore between 10 and 15 GWh of electricity. Instead, the onshore EP wind profile ranges between 4 and 7 m/s, generating a limited but steady power in winter season, thanks to the large amount of onshore turbines installed. However, production falls in the summer season because the average wind speed is only slightly higher or equal to the onshore turbines' cut-in wind speed. Instead, the ES scenario production reaches the highest peaks for both onshore and offshore wind turbines, due to the copious amount of hours with wind speed well above 10 m/s and 15 m/s, as reported by Figure A.1; therefore, electricity generation has peaks on the same order of the maximum electricity demand (Figure A.3a). On the one hand, the spikes' integration of the ES scenario allows the RES production to rise, on the other hand the abundant negative spikes determine discontinuity along the yearly production. About 10% of offshore wind is below cut-in wind speed, and for onshore wind the rate rises at 25%. With lower amount of turbines, the offshore production is strongly affected by negative peaks during the summer season, with production over 90% lower than winter season, excluding few peaks hours.

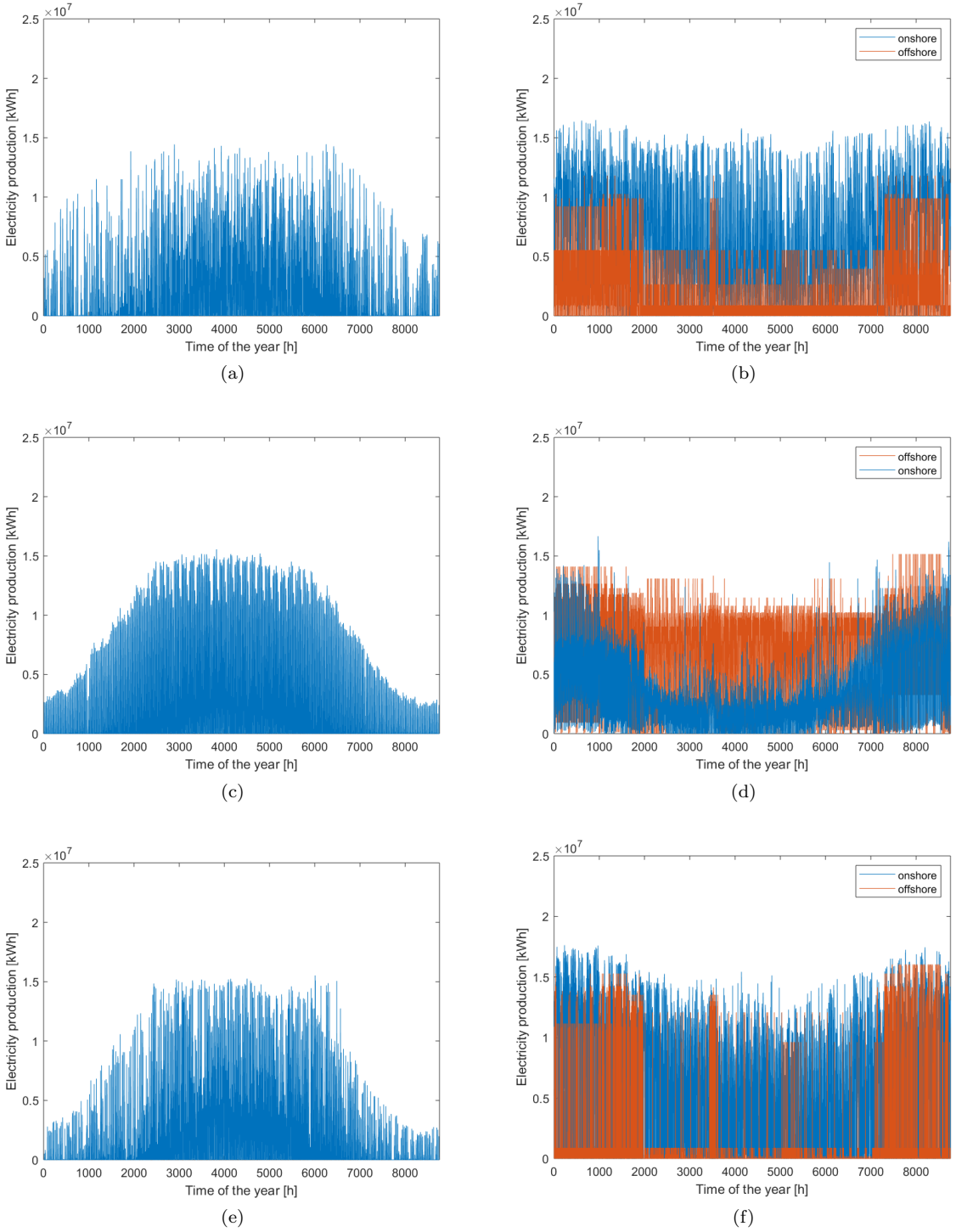

Figure 8.1: Power production for RD profiles, with solar PV (a) and off/onshore wind turbines (b); for EP profiles, with solar PV (c) and off/onshore wind turbines (d); for ES profiles, with solar PV (e) and off/onshore wind turbines (f).

Same type of considerations can be made about solar PV production. Although the maximum power produced is on the same dimension for all three scenarios, the EP scenario produces 10% more of solar power, due to steadier solar radiation.

8.2 Energy storage

Energy storage for RD scenario is characterised by an accumulation of energy during the first part of the year, then by a distinctive depletion of energy from the 2000th hour, as depicted by Figure 8.2a, Figure 8.3a and Figure 8.3b. Figure 8.3a shows a conspicuous amount of peaks along all year applied for hydrogen conversion. Until hour 2000, the intense blue depicts stronger electricity input. Instead, Figure 8.3b shows the electricity produced via the PEM fuel cells by drawing hydrogen from the salt cavern; extra production other than NDRES is required between hour 2000 and around 3500, because the offshore wind production halves from its original path (Figure 8.1b). The following offshore peak production, around the 3500th hour, is sent to storage, as shown by the darker blue in Figure 8.3a and the relative peak reaching 2.4347e+07 in Figure 8.2a. The stored energy is then approximately constant until hour 5500, even with minimum wind production. Presumably, substantial summer solar radiation is sent to load, partially compensating for lower wind production. However, violation is also copious during summer season. Around the 700th hour, solar PV power production decreases and both onshore and offshore production intensify, refilling the salt cavern with hydrogen. The operation of the PEMFC during the year strictly follows the hydrogen cycle in the salt caverns; during winter time the wind energy overproduced is stored, and no energy is sent to the grid. Also, most of the variation of the stored energy develop in a short time-interval of about 1000 hours, when offshore wind production drops and solar radiation is not intensive enough yet to (partially) compensate for it.

Energy storage in the salt caverns for EP scenario follows the path as shown by Figure 8.2b. As above mentioned, the electricity entering the electrolyser is abundant for EP scenario due to the steady electricity production; the winter on/offshore wind overproduction is accumulated during the first part of the year; just before the 2000th hour, the hydrogen flow decreases as the onshore and offshore production decrease, the latter rises again until hour 3000. From the 3000th hour of the year to the 7000th the energy stored arrives at the minimum, accordingly to the offshore and onshore power production. Although, a relative peak is recorded around the 5000th hour, due to a slight increase is solar PV power and few wind production spikes. Subsequently, the energy stored rises with the growth of onshore and offshore production.

Energy stored for the ES scenario begins the year by varying from maximum amount of energy stored to minimum, around the 1000th hour. During this period the onshore production experiences over one fifth of the hours with no generation, due to the corresponding negative peaks modelled. The negative peaks for offshore wind profiles fewer than the onshore counterpart, but still conspicuous; also, the demand for electricity is in that period at highest values. Therefore, the overall grid is balance by increasing violation (Figure A.3d) and by employing the stored energy. However, the amount of energy produced by the PEMFC reaches maximum of 500 kWh, the 3.3e-03% of the average hourly demand, due to the limited size deployed. Hydrogen flow entering the salt cavern subsequently increases, as shown by the intense blue in Figure 8.3e between hour 1000 and 2000, and by the rise of the stored energy in Figure 8.2a. Accordingly, offshore power generation is larger. Then, it drastically drops around the 2000th hour, only partially compensated by an increase solar produced power and through PEMFC, although very limited by the capacity installed. From hour 3500, peaks of power produced with all NDRES technologies, reaching intensities of 1.5e+07 kWh, allow the stored energy to slowly rise; the peaks are clearly visible from Figure 8.3e, showing the electricity sent for hydrogen conversion. The growth intensifies with the coming of higher and steadier offshore winter wind.

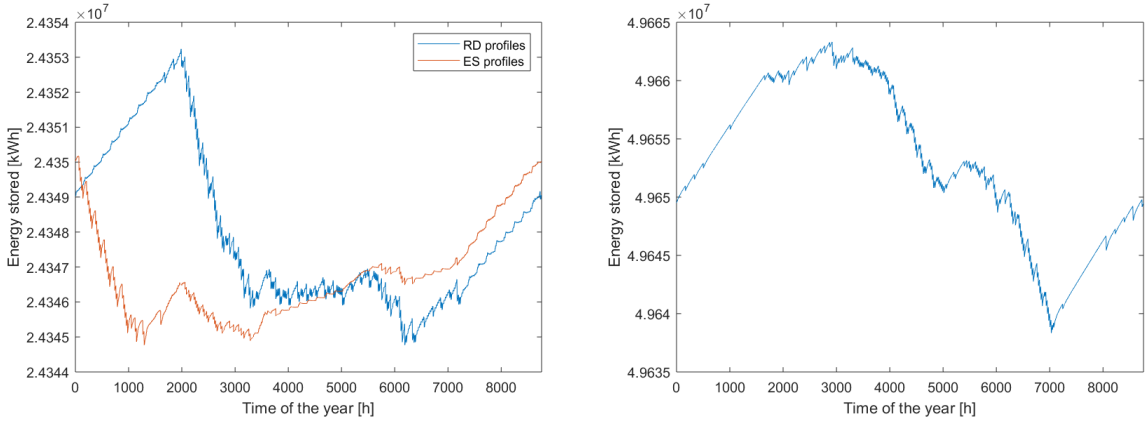

(a) (b)

Figure 8.2: Energy stored in salt caverns along the year for RD (a), ES (a) and EP (b).

8.3 Variation of offshore area available for wind turbine installations

The following results compared the henceforth called *Baseline* ES scenario, previously analysed, to scenario *ES200*, with area availability for wind turbine installations increased by 200%. Optimal technology deployment for baseline ES and ES200 differs for the amount WT9500 installed, increased in the same order as the area, and PEMFC, not installed for the new scenario. Table 8.3 reports the total units installed. Presumably, the increased offshore production compensate for the very limited electricity previously re-sent to grid from the storage (Figure 8.3f).

From a comparison between Figure 8.4b and Figure 8.1f, it appears that the lower visible production, distinctive in the summer season, has increased in comparison to the baseline scenario; it approximately triplicate, due to the triple amount of turbines producing power at limited wind speeds. However, the maximum offshore production does not variate, suggesting power curtailment. Table 8.4 shows that the overall level of autarky reached, by largely increasing the constraint on amount of wind turbine installed, does not increases as expected. Furthermore, the electricity supplied by offshore production only slightly increases, presumably due to power curtailment. Although, solar PV power almost double for ES200 scenario; it is then probable that baseline scenario experiences power curtailment for solar PV, as

Table 8.3: Technology deployment with 3 nodes optimisation and ES scenarios, with baseline offshore technical potential and increasing it by 200%. Wind turbine unit is amount of turbines [#], solar PV unit is $[m^2]$, PEME, PEMFC and H2 in $[kW]$.

Technologies	Unit	ES	ES200
WT1500	#	0	0
WT2500	#	0	0
WT4500	#	8109	8109
WTex (onshore)	#	40	40
WT6000	#	0	0
WT9500	#	3692	11077
WTex (offshore)	#	0	0
solar PV	m^2	2e+08	2e+08
PEME	kW	100	100
H2 storage	kW	196349	196349
PEMFC	kW	500	0

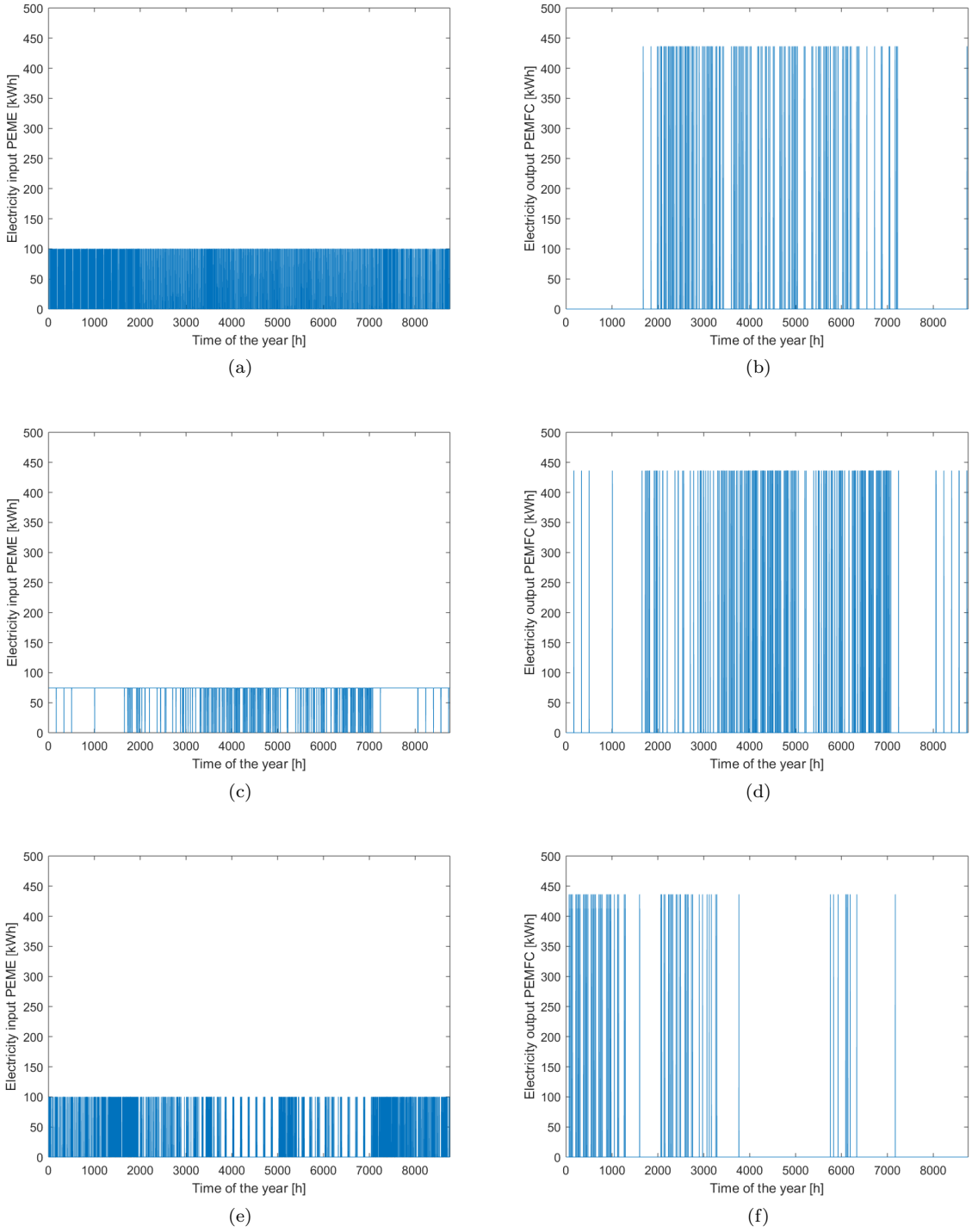

Figure 8.3: Power applied to electrolysis via PEME for RD profiles (a), EP profiles (c) and ES profiles (e); power produced from hydrogen via PEMFC for RD profiles (b), EP profiles (d) and ES profiles (f).

solar radiation and capacity installed do not vary for the two scenarios. To conclude, a comment about PtG system; for ES200 scenario PEME is installed, converting electricity into hydrogen and storing it in salt caverns. For the scenario in analysis PEME operation differs; ES200 scenario accumulates hydrogen in the first part of the year (Figure 8.4c), as expected due to the winter higher and steadier winds, and opposite to ES behaviour. However, Figure 8.4d depicts a depletion of the hydrogen stored after the 2000th, even if the carrier cannot be re-converted in electricity as no PEMFC is installed. Therefore,

Table 8.4: Level of autarky and ratio of demand supplied with wind turbines, PV or storage technologies with ES and ES200 methods.

	ES	ES200
Autarky	69.5%	70.4 %
Wind turbines onshore production	49.6 %	39.6 %
Wind turbines offshore production	7.9 %	9.6 %
solar PV production	12.0 %	21.2 %
PEMFC production	3.9e-05 %	0 %

dissipation may represent the cause of energy consumption from the stored hydrogen, as shown in Figure 8.4e around hour 2000.

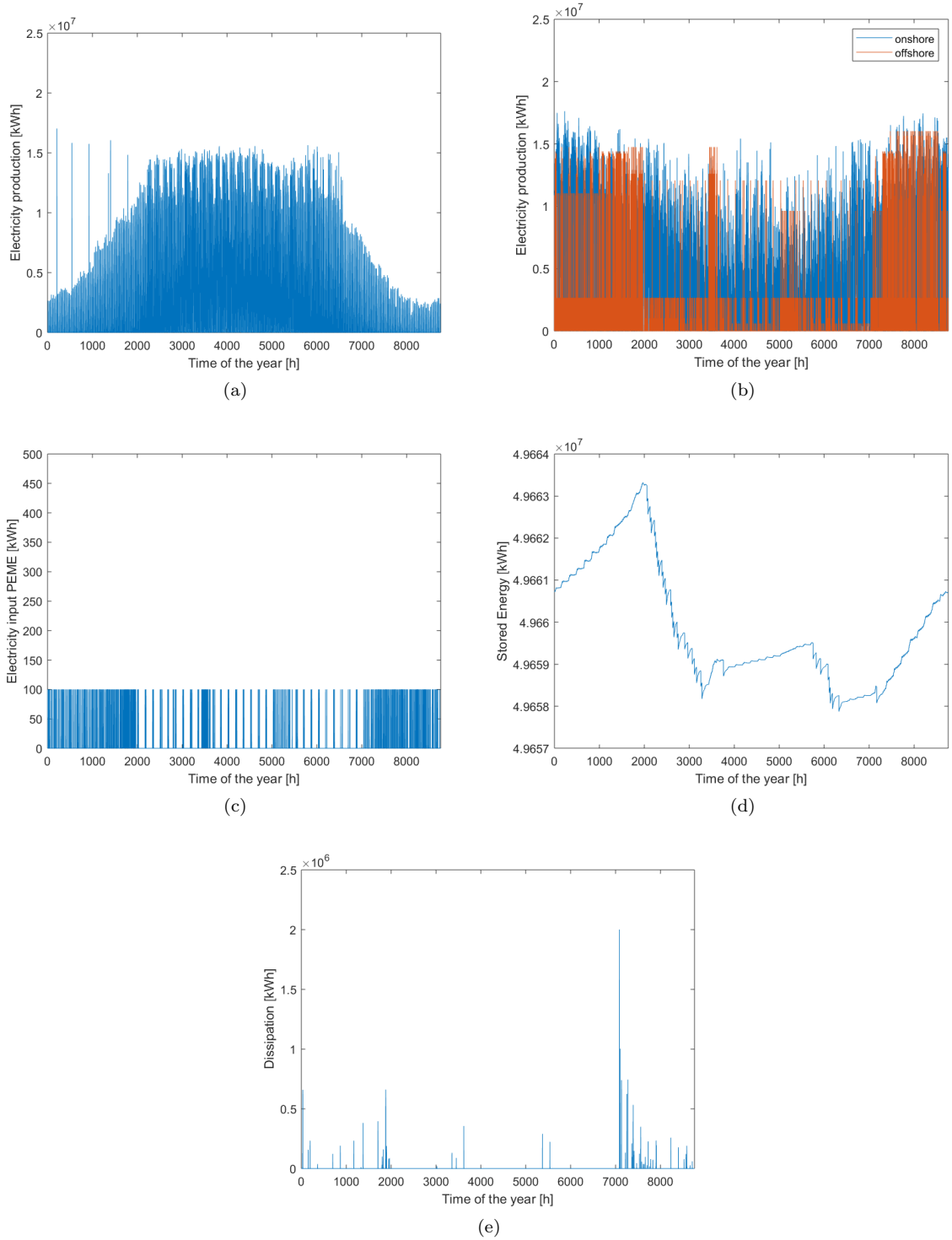

Figure 8.4: ES scenario with offshore area increased by 200% results; solar PV production (a), onshore and offshore wind turbines production (b), electricity converted in hydrogen (c), energy stored in salt cavern (d) and electricity dissipated (e).

Chapter 9

Discussion

The previous chapter shows a great alteration of the optimal outcome by varying wind speed and solar radiation profiles. Although optimal system design only slightly changes, the modality of operation of the electric grid presents difference on the order of tens percentage of the load. Therefore, a critical analysis of the methods carried out is essential.

The RD method is one of the most widely used in the context of employing long-term database to create a TMY. Although, the original approach of selecting 12 typical months is modified in this research for the selection of 365 typical days. So, the periods with real sequences of data are limited to 24, which likely reduce verisimilitude of system operations for two reasons; application of typical month is most likely to present real magnitude of spikes than a typical day, and longer real sequences of data may describe the intermittency problematic more realistically. The ES method presents substantial limitations on this matter; the random integration of negative and positive spikes does not allow the creation of realistic sequences. In fact, results show the poor representation of steady wind profile during the winter season, to a point that it causes the hydrogen stored to diminish during the first trimester of the year, as opposite to the other results.

The methods applied for the case-studies present limitations in the context of system discretisation. In fact, as weather profiles are proved to be relevant, the spatial average performed between data of various weather stations could lead to inappropriate values. Additionally, overall costs input may have influence on the outcomes, as they govern the optimisation. On the one hand, NDRES are deployed to their full potential for all the simulations, suggesting their realistic current economic accessibility. On the other hand, the data retrieved could be improved by many means, particularly for the more uncertain offshore installation costs (i.e. introducing economy of scale on project size, retrieving current and case-specific data). As regards to PEME and PEMFC, these are deployed to a degree insignificant to the overall system balance. This suggests that technical potential of large-scale storage with PtG may be hindered by economic feasibility. In fact, despite the triplication of offshore wind turbine capacity, PtG is not oversized but the opposite. Rather, power curtailment is applied. So, the potential of integrating NDRES to the grid on the order of hundreds of GW may be hindered by the widely applied power curtailment. For a better understanding on this matter, multiple simulations were planned; however the analysis was limited by a last minute collection of the results and computational problematics arising with the EHub. To conclude, it must be noted the case-specificity of the results in relation to the boundaries of the system tested. In fact, influential data of weather profiles and area constraints are strictly valid for the Netherlands, as well as the potential of hydrogen storage with the modality analysed, which requires the particular geological formation of salt cavern.

Chapter 10

Conclusion and recommendations for further research

The presented research aims at evaluating to what degree does the modelling method for generating a TMY influences design and operation of the Dutch electric grid, where NDRES are coupled with large-scale, hydrogen storage. The research is carried out in the context of MILP energy system modelling by applying the EHub, framework created by [Gabrielli et al., 2018, Weimann et al., 2019]. The EHub calls for the input of hourly data on a year time horizon.

As the utilisation of a singular year is not appropriate, three methodologies are developed for the generation of a TMY from a long-term database, with hourly resolution on a one-year time horizon. RD represents a modified version of a widely used method, EP calculates the hourly expected values from the long-term database and ES integrates EP with the expected number of positive and negative spikes, with spike magnitude in accordance to the probability distribution of the their amplitude. Subsequently, three scenarios are analysed; the TMY generated are employed for the optimisation of the Dutch grid to assess both the EHub and the methods for TMY. Regarding the latter, advantages and disadvantages of the mentioned emerge. RD method calculates realistic sequences of weather data; however, the magnitude of the profiles' spikes are limited. Improvement potential lays on the calculation of representative weeks or months, rather than days. In such manner, the spikes' amplitude may increase. Instead, EP method emerges as inadequate; the problem of intermittency is completely hindered by the use of expected values; the EP scenario shows that power is constantly produced and NDRES operate such a base-load on the system. ES methodology improves EP by means of the integration of positive and negative spikes. On the one hand, expected spikes' frequencies and probable amplitudes create profiles with realistic magnitudes; on the other hand, the random insertion of spikes creates an unrealistic data sequence and causes inappropriate operation when storage is deployed. The method could be improved by modifying the random insertion to generate statistically expected sequences.

28-nodes simulations were attempted but not terminated due to computational complications. Therefore, simulations with a lower degree of discretisation are carried out. The results of the 3-nodes case-studies show that by varying method for TMY, optimal design variates on a small scale and system operation differs to a large extent; offshore generation is the most affected outcome, together with hydrogen stored in salt caverns. Although, the latter is less relevant because its extent in all the scenarios is negligible in proportion to the total load supplied. Onshore power production is larger than the offshore counterpart; their trade-off seems unrealistic, taking into consideration the rates of offshore installations carried out in recent years throughout the North Sea [4C,]. The feature of continuous curtailment hinders the actual offshore generation potential and further research shall be performed by applying

discrete curtailment as reported by [Weimann et al., 2019]; wind turbines shall more realistically be turned off or adhere to their power curves. Furthermore, continuous power curtailment hinders the actual potential of PtG storage system, as only a limited amount of excess power is currently stored. The propensity of curtailing rather than storing is in line with current trends, due to current storage cost. Further research shall be made to analyse whether storing would prevail curtailing if an emissions minimisation approach is carried out instead of a costs approach.

Bibliography

[4C,] 4C Offshore Overview - 4C Offshore. https://www.4coffshore.com/. Last accessed: 2019-03-14.

[MHI,] MHI Vestas Offshore Wind. http://www.mhivestasoffshore.com/. Last accessed: 2019-01-10.

[dem,] regelleistung.net - Internetplattform zur Vergabe von Regelleistung. https://www.regelleistung.net/ext/tender/. Last accessed: 2018-10-01.

[Hal,] World's Largest Offshore Wind Turbine — Haliade-X — GE Renewable Energy. https://www.ge.com/renewableenergy/wind-energy/turbines/haliade-x-offshore-turbine. Last accessed: 2019-03-14.

[Barbir, 2009] Barbir, F. (2009). Transition to renewable energy systems with hydrogen as an energy carrier. *Energy*, 34(3):308–312.

[Bilgili et al., 2011] Bilgili, M., Yasar, A., and Simsek, E. (2011). Offshore wind power development in Europe and its comparison with onshore counterpart. *Renewable and Sustainable Energy Reviews*, 15(2):905–915.

[Blanco, 2009] Blanco, M. I. (2009). The economics of wind energy. *Renewable and Sustainable Energy Reviews*, 13:1372–1382.

[Castillo and Gayme, 2014] Castillo, A. and Gayme, D. F. (2014). Grid-scale energy storage applications in renewable energy integration: A survey. *Energy Conversion and Management*, 87.

[Cengel and Boles, 2015] Cengel, Y. A. and Boles, M. A. (2015). *Thermodynamics: An Engineering Approach, Eigth Edition*. McGraw-Hill Education.

[Centraal Bureau voor de Statistiek,] Centraal Bureau voor de Statistiek. CBS StatLine. https://statline.cbs.nl/Statweb/. Last accessed: 2019-01-21.

[Defaix et al., 2012] Defaix, P. R., van Sark, W. G., Worrell, E., and de Visser, E. (2012). Technical potential for photovoltaics on buildings in the EU-27. *Solar Energy*, 86(9):2644–2653.

[Díaz-González et al., 2012] Díaz-González, F., Sumper, A., Gomis-Bellmunt, O., and Villafáfila-Robles, R. (2012). A review of energy storage technologies for wind power applications. *Renewable and Sustainable Energy Reviews*, 16(4):2154–2171.

[ECN,] ECN. Renewable energy: current Dutch policy is falling short of 2020 target despite strong growth. https://www.ecn.nl/nl/nieuws/item/renewable-energy-current-dutch-policy-is-falling-short-of-2020-target-despite-strong-growth/. Last accessed: 2019-03-10.

[EuroPages,] EuroPages. Index, Netherlands, companies. https://www.europages.co.uk/companies/Netherlands/. Last accessed: April 2014.

[European Commission,] European Commission. Europe 2020 targets: statistics and indicators for the Netherlands. https://ec.europa.eu/info/business-economy-euro/economic-and-fiscal-policy-coordination/eu-economic-governance-monitoring-prevention-correction/european-semester/european-semester-your-country/netherlands/europe-2020-targets-statistics-and-indicators-neth. Last accessed: 2019-03-10.

[European Environmental Agency, 2009] European Environmental Agency (2009). Europe's onshore and offshore wind energy potential. Technical Report 6.

[Finkelstein and Schafer, 1971] Finkelstein, J. M. and Schafer, R. E. (1971). Improved goodness-of-fit tests. *Biometrika*, 58(3):641–645.

[Gabrielli et al., 2018] Gabrielli, P., Gazzani, M., Martelli, E., and Mazzotti, M. (2018). Optimal design of multi-energy systems with seasonal storage. *Applied Energy*, 219(May 2017):408–424.

[Guan, 2009] Guan, L. (2009). Preparation of future weather data to study the impact of climate change on buildings. *Building and Environment*, 44(4):793–800.

[Gurobi,] Gurobi. Mixed-Integer Programming (MIP) - A Primer on the Basics. http://www.gurobi.com/resources/getting-started/mip-basics. Last accessed: 2019-03-10.

[Hadjipaschalis et al., 2009] Hadjipaschalis, I., Poullikkas, A., and Efthimiou, V. (2009). Overview of current and future energy storage technologies for electric power applications. *Renewable and Sustainable Energy Reviews*, 13:1513–1522.

[Hawkes and Leach, 2009] Hawkes, A. D. and Leach, M. A. (2009). Modelling high level system design and unit commitment for a microgrid. *Applied Energy*, 86(7-8):1253–1265.

[Hof et al., 2012] Hof, A., Brink, C., Mendoza Beltran, A., and den Elzen, M. (2012). *Greenhouse Gas Emission Reduction Targets for 2030. Conditions for an EU target of 40%.*

[Iea Wind,] Iea Wind. Data Viewer - Task26. https://community.ieawind.org/task26/dataviewer. Last accessed: 2019-03-10.

[Junginger, 2005] Junginger, H. (2005). *Learning in Renewable Energy Technology Development.* PhD thesis.

[Kaldellis et al., 2016] Kaldellis, J., Apostolou, D., Kapsali, M., and Kondili, E. (2016). Environmental and social footprint of offshore wind energy. Comparison with onshore counterpart. *Renewable Energy*, 92:543–556.

[KNMI, a] KNMI. Uurgegevens van het weer in Nederland - Download. https://projects.knmi.nl/klimatologie/uurgegevens/selectie.cgi. Last accessed: 2019-03-10.

[KNMI, b] KNMI. Uurgegevens van Noordzee stations. https://www.knmi.nl/nederland-nu/klimatologie/uurgegevens{_}Noordzee. Last accessed: 2019-03-10.

[Kono et al., 2017] Kono, J., Ostermeyer, Y., and Wallbaum, H. (2017). The trends of hourly carbon emission factors in Germany and investigation on relevant consumption patterns for its application. *International Journal of Life Cycle Assessment*, 22(10):1493–1501.

[Madow, 1968] Madow, W. G. (1968). Elementary Sampling Theory. In *Technometrics*, volume 10, pages 621–622.

[Mancarella, 2014] Mancarella, P. (2014). MES (multi-energy systems): An overview of concepts and evaluation models. *Energy*, 65:1–17.

[Marnay et al., 2008] Marnay, C., Venkataramanan, G., Stadler, M., Siddiqui, A. S., Firestone, R., and Chandran, B. (2008). Optimal Technology Selection and Operation of Commercial-Building Microgrids. *IEEE Transactions on Power Systems*, 23(3):975–982.

[McKenna et al., 2015] McKenna, R., Hollnaicher, S., Ostman, P., and Fichtner, W. (2015). Cost-potentials for large onshore wind turbines in Europe. *Energy*, 83:217–229.

[Mehleri et al., 2013] Mehleri, E. D., Sarimveis, H., Markatos, N. C., and Papageorgiou, L. G. (2013). Optimal design and operation of distributed energy systems: Application to Greek residential sector. *Renewable Energy*, 51:331–342.

[MHI Vestas Offshore,] MHI Vestas Offshore. MHI Vestas Inks Firm Order for Borssele V Innovation Site. http://www.mhivestasoffshore.com/mhi-vestas-inks-firm-order-borssele-v-innovation-site/. Last accessed: 2019-01-10.

[Michalski et al., 2017] Michalski, J., Bu, U., Crotogino, F., and Donadei, S. (2017). Hydrogen generation by electrolysis and storage in salt caverns: Potentials, economics and systems aspects with regard to the German energy transition. *ScienceDirect*, 2(89).

[Morvaj et al., 2016] Morvaj, B., Evins, R., and Carmeliet, J. (2016). Optimization framework for distributed energy systems with integrated electrical grid constraints. *Applied Energy*, 171:296–313.

[Ozarslan, 2012] Ozarslan, A. (2012). Large-scale hydrogen energy storage in salt caverns. *International Journal of Hydrogen Energy*, 37:14265–14277.

[Poluzzi, 2017] Poluzzi, A. (2017). Modeling, simulation and optimization of hydrogen storage in salt caverns.

[Pudjianto et al., 2014] Pudjianto, D., Aunedi, M., Djapic, P., and Strbac, G. (2014). Whole-Systems Assessment of the Value of Energy Storage in Low-Carbon Electricity Systems. *IEEE Transactions on Smart Grid*, 5(2):1098–1109.

[Rhodes, 2016] Rhodes, C. J. (2016). Current Commentary. The 2015 Paris Climate Change Conference: COP21. *Science Progress*, 99(1):97–104.

[Ribeiro et al., 2001] Ribeiro, P., Johnson, B., Crow, M., Arsoy, A., and Liu, Y. (2001). Energy storage systems for advanced power applications. In *Proceedings of the IEEE*, volume 89, pages 1744–1756.

[Salameh and Salameh, 2014] Salameh, Z. and Salameh, Z. (2014). Energy Storage. *Renewable Energy System Design*, pages 201–298.

[Samsatli et al., 2015] Samsatli, S., Staffell, I., and Samsatli, N. J. (2015). Optimal design and operation of integrated wind- hydrogen-electricity networks for decarbonising the domestic transport sector in Great Britain. *International Journal of Hydrogen Energy*, 41(1):447–475.

[Shao et al., 2017] Shao, C., Wang, X., Shahidehpour, M., Wang, X., and Wang, B. (2017). An MILP-Based Optimal Power Flow in Multicarrier Energy Systems. *IEEE Transactions on Sustainable Energy*, 8(1):239–248.

[Siemens, a] Siemens. Siemens 6.0 MW Offshore Wind Turbine. www.siemens.com/wind. Last accessed: 2019-01-10.

[Siemens, b] Siemens. Wind Turbine SWT-2.5-120. Technical report.

[SolarSolutions, 2018] SolarSolutions (2018). Dutch Solar Trend Report 2018. http://www.solarsolutions.nl/download/.

[te Raa et al., 2010] te Raa, H., Ockels, W., Melkert, J., Snijders, T., and Beelaerts and Blokland, W. (2010). Bio jet fuel from macro algae. Technical report.

[TenneT, 2018] TenneT (2018). TenneT Market Review 2017 – Electricity market insights.

[The Ministry of Infrastructure and the Environment, 2014] The Ministry of Infrastructure and the Environment (2014). White Paper on Offshore Wind Energy. Technical report.

[The World Bank,] The World Bank. Arable land (% of land area) — Data. https://data.worldbank.org/indicator/AG.LND.ARBL.ZS?view=chart. Last accessed: 2018-10-15.

[TNO,] TNO. Potentieel opslag in zoutcavernes. https://www.tno.nl/en/. Last accessed: April 2014.

[turbine models.com,] turbine models.com, W. Vestas V120-4.5. https://en.wind-turbine-models.com/turbines/1728-vestas-v120-4.5. Last accessed: 2019-03-10.

[Twidell and Weir, 2015] Twidell, J. and Weir, T. (2015). *Renewable Energy Resources. Third Edition.* Routledge.

[Van der Zwaan et al., 2012] Van der Zwaan, B., Rivera-Tinoco, R., Lensink, S., and van den Oosterkamp, P. (2012). Cost reductions for offshore wind power: Exploring the balance between scaling, learning and R&D. *Renewable Energy*, 41:389–393.

[Van Sark, W.G.J.H.M.; Schoen, 2016] Van Sark, W.G.J.H.M.; Schoen, T. (2016). Photovoltaic system and components price development in the Netherlands. In *33rd European Photovoltaic Solar Energy Conference and Exibition*, pages 2866–2869.

[Voormolen et al., 2016] Voormolen, J. A., Junginger, H. M., and van Sark, W. G. J. H. M. (2016). Unravelling historical cost developments of offshore wind energy in Europe. *Energy Policy*, 88:435–444.

[Weimann et al., 2019] Weimann, L., Gabrielli, P., Boldrini, A., Kramer, G. J., and Gazzani, M. (2019). On the role of H_2 storage and conversion for wind power-production in the Netherlands. In *Proceedings of the 29th European Symposium on Computer Aided Process Engineering.*

[Welder et al., 2018] Welder, L., Ryberg, D. S., Kotzur, L., Grube, T., Robinius, M., and Stolten, D. (2018). Spatio-temporal optimization of a future energy system for power-to-hydrogen applications in Germany. *Energy*, 158:1130–1149.

[Wilks and Wilby, 1999] Wilks, D. S. and Wilby, R. L. (1999). The weather generation game: a review of stochastic weather models. *Progress in Physical Geography*, 23(3):329–357.

[Windstats,] Windstats. Statistieken. https://windstats.nl/statistieken/. Last accessed: 2018-10-15.

[Wiser et al., 2016] Wiser, R., Jenni, K., Seel, J., Baker, E., Hand, M., Lantz, E., and Smith, A. (2016). Expert elicitation survey on future wind energy costs. *Nature Energy*, 1(10).

[Wouters et al., 2015] Wouters, C., Fraga, E. S., and James, A. M. (2015). An energy integrated , multi-microgrid, MILP (mixed-integer linear programming) approach for residential distributed energy system planning - A South Australian case-study. *Energy*, 85:30–44.

[Yang et al., 2003] Yang, H., Lu, L., and Burnett, J. (2003). Weather data and probability analysis of hybrid photovoltaic–wind power generation systems in Hong Kong. *Renewable Energy*, 28(11):1813–1824.

[Zang et al., 2012] Zang, H., Xu, Q., Du, P., and Ichiyanagi, K. (2012). A Modified Method to Generate Typical Meteorological Years from the Long-Term Weather Database. *International Journal of Photoenergy*, 2012:9.

Appendix A

Weather profiles

Table A.1: 28-nodes discretisation: weather stations used the creation of wind speed and solar radiation profiles database, for province nodes [KNMI, b].

Province node	Weather stations
Drenthe	279, 280
Flevoland	258, 269, 273
Fryslan	242, 267, 270
Gelderland	275, 283, 356
Groningen	277, 285, 286
Limburg	377, 380, 391
Noord-Brabant	340, 350, 370, 375
Noord-Holland	235, 240, 248, 249, 251
Overijssel	278, 290
Utrecht	260, 348
Zeeland	308, 310, 312, 313, 315, 316, 319, 323, 324, 331
Zuid-Holland	215, 330, 343, 344

Table A.2: 28-nodes discretisation: weather stations used for the creation of wind speed profiles database for the offshore nodes, with the distances applied in the calculation of the weighted average velocity [KNMI, a].

Offshore nodes	Weather stations	Distances (in order)
OS North Wadden Island	214	-
OS Holland Coast	203, 321, 320, 212	45, 63, 52, 67
OS Borssele	321, 320	37, 41
OS IJmuiden Ver	203, 212, 252	50, 39, 57

Table A.3: 3-nodes discretisation: weather stations used the creation of wind speed and solar radiation profiles database [KNMI, b, KNMI, a].

Nodes	Weather stations
Onshore	235, 260, 290, 310, 380
Offshore	206, 212, 321

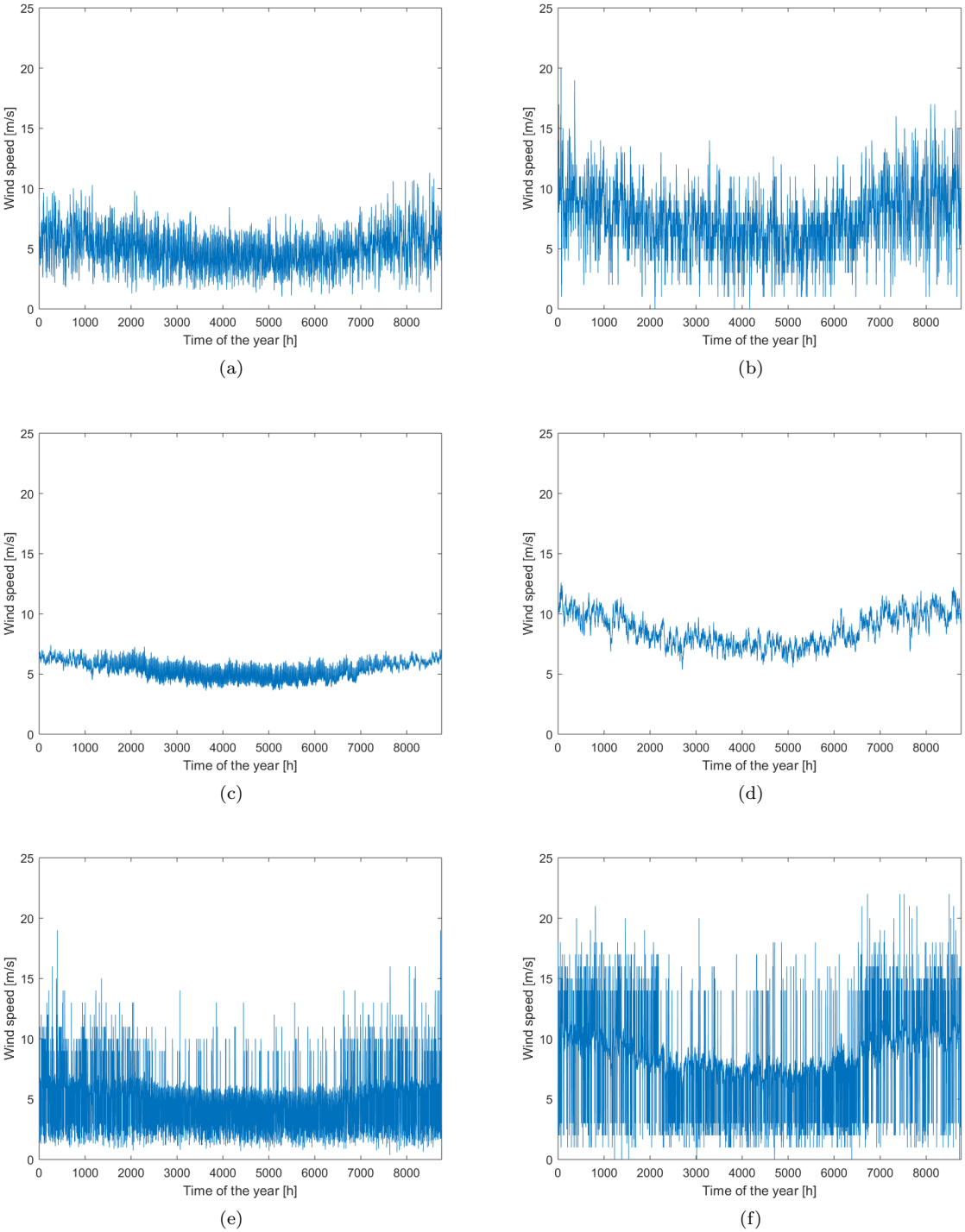

Figure A.1: Onshore and offshore wind profile calculated with the method of RD, respectively (a) and (b), EP method, respectively (c) and (d) and ES method, (e) and (f).

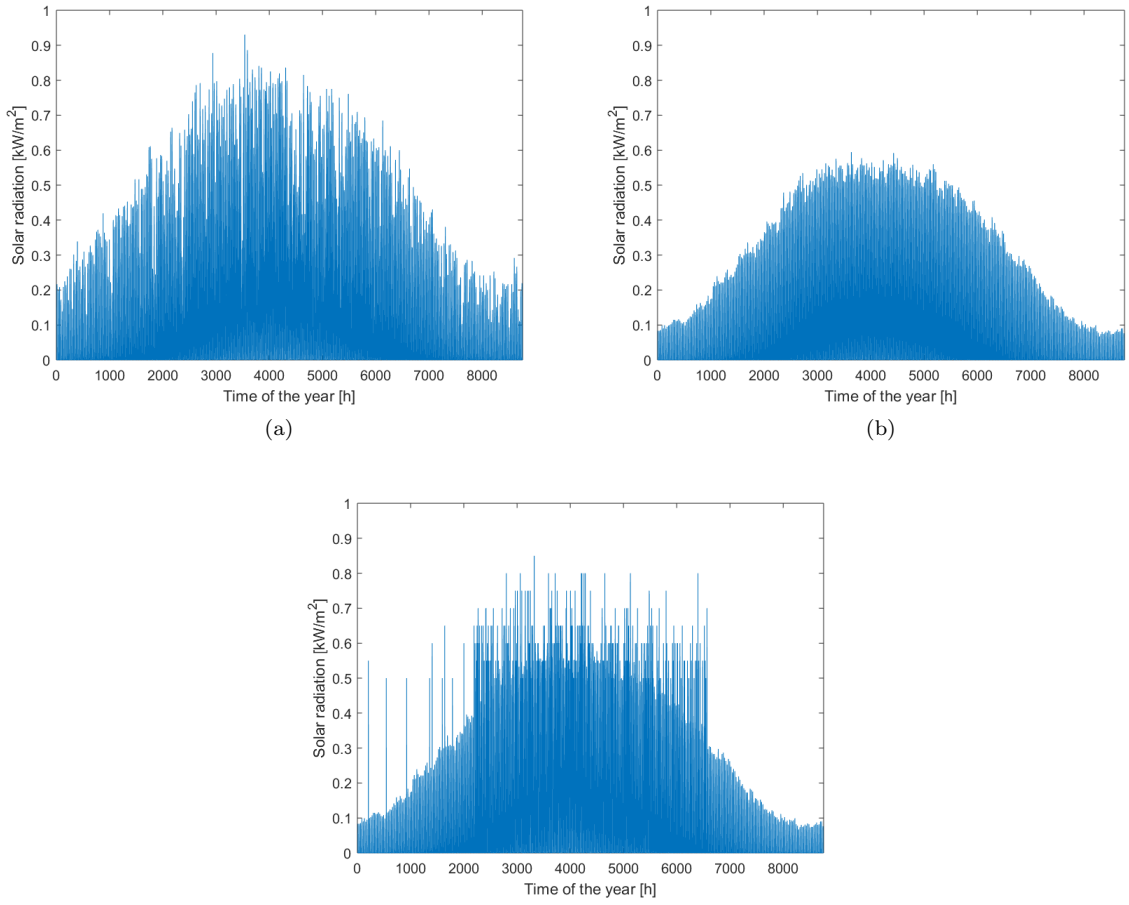

(a) (b)

(c)

Figure A.2: Solar radiation calculated with the method of RD (a), EP (b) and ES method (c).

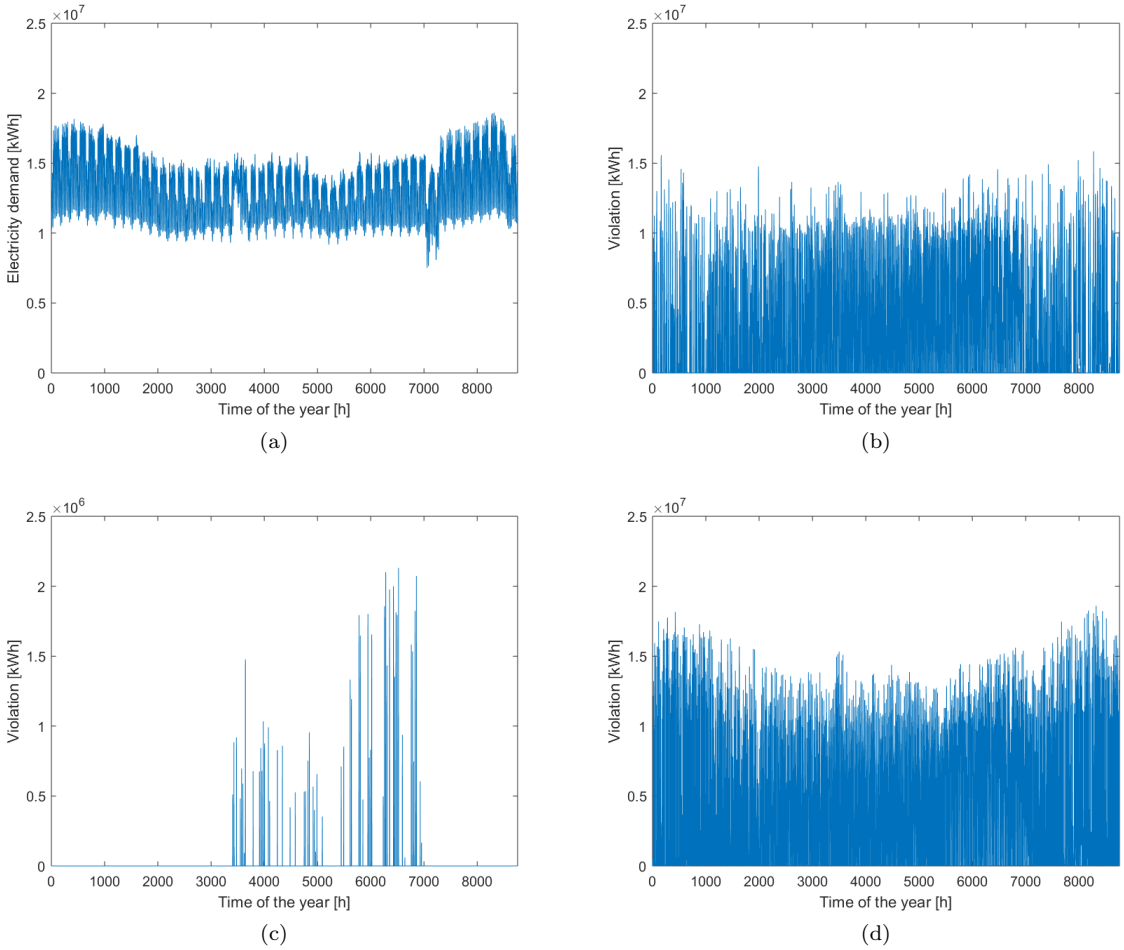

Figure A.3: Power production for RD profiles, with solar PV (a) and off/onshore wind turbines (b); for EP profiles, with solar PV (c) and off/onshore wind turbines (d); for ES profiles, with solar PV (e) and off/onshore wind turbines (f).

Appendix B

Input data

Table B.1: List of nodes, space availability constraints and annual electricity demand.

Nodes	Land available WT $[km^2]$	Sea available WT $[km^2]$	Rooftop available PV $[km^2]$	Electricity demand $[kWh/year]$
Drenthe	402	-	8.57	5.13e+09
Flevoland	362	-	4.92	2.19e+09
Fryslan	862	-	9.95	3.79e+09
Gelderland	770	-	26.1	1.28e+10
Groningen	444	-	9.07	7.93e+09
Limburg	332	-	16.64	9.01e+09
Noord-Brabant	762	-	34.17	1.56e+10
Noord-Holland	614	-	25.16	1.55e+10
Overijssel	513	-	14.49	6.76e+09
Utrecht	217	-	12.66	6.66e+09
Zeeland	440	-	6.58	2.43e+09
Zuid-Holland	513	-	31.68	2.72e+10
OS North Wadden Island	-	1210	-	-
OS Holland Coast	-	165	-	-
OS Borssele	-	380	-	-
OS IJmuiden Ver	-	1145	-	-
SC Ternaard	-	-	-	-
SC Pieterburen	-	-	-	-
SC Hoogezand	-	-	-	-
SC Winschoten	-	-	-	-
SC Zuidwending	-	-	-	-
SC Anloo	-	-	-	-
SC Ontswedde	-	-	-	-
SC Boertange	-	-	-	-
SC Gasselte-Drouwen	-	-	-	-
SC Hooghalen	-	-	-	-
SC Schoonloo	-	-	-	-
SC Hoogeveen	-	-	-	-